

PAPER TITLE:

A general framework and related procedures for multiscale analyses of DInSAR data in subsiding urban areas

Authors:

Leonardo Cascini*, Dario Peduto*, Livia Arena*, Settimio Ferlisi*, Gianfranco Fornaro**, Diego Reale**

* Department of Civil Engineering

University of Salerno, Italy

Via Giovanni Paolo II, 132

84084 - Fisciano (SA), Italy

E-mail: l.cascini@unisa.it; dpeduto@unisa.it; sferlisi@unisa.it; liarena@unisa.it

**

Institute for Electromagnetic Sensing of the Environment (IREA – CNR)

Via Diocleziano 328

80124 Naples, ITALY

E-mail: fornaro.g@irea.cnr.it; reale.d@irea.cnr.it

Corresponding author

Dario Peduto

Department of Civil Engineering

University of Salerno

Via Giovanni Paolo II, 132

84084 - Fisciano (SA)

Email: dpeduto@unisa.it

Tel. +39 089 964120

Mobile +39 3286935656

HIGHLIGHTS

A general framework for the use of DInSAR data is presented.

Procedures for multiscale analysis of multisensor DInSAR data in subsiding **urban** areas are shown.

Applications for **different sites of** Campania region (southern Italy) **are shown at different scales.**

The procedures can address consequence analyses to the facilities at subsidence risk.

The damages recorded in the test sites confirm the obtained results.

Abstract

In the last decade Differential Synthetic Aperture Radar (DInSAR) data were successfully tested in a number of case studies for the detection, mapping and monitoring of ground displacements associated with natural or anthropogenic phenomena. More recently, several national and regional projects all around the world provided rich data archives whose confident use, however, should rely on multidisciplinary **experts** in order to avoid misleading interpretations. To this aim, the present work **first** introduces a general framework for the use of DInSAR data; then, focusing on the analysis of subsidence phenomena and the related consequences to the exposed facilities, a set of original procedures is proposed. By drawing a multiscale approach the study highlights the different goals to be pursued at different scales of analysis via high/very high resolution SAR sensors and presents the results with reference to the case study of the Campania region (southern Italy) where widespread ground displacements occurred and damages of different severity were recorded.

1 Introduction

In the last decade images acquired by Synthetic Aperture Radar (SAR) sensors and processed via Differential Interferometry algorithms (DInSAR) have been increasingly applied by the scientific community to study the measurable effects of natural or anthropogenic phenomena (or dangers) in different fields of Geosciences – including Geology, Geophysics and Glaciology (Crosetto et al., 2003) – as well as in the Civil and Environmental Engineering. This is essentially due to several advantages offered by DInSAR techniques, such as: the possibility of measuring ground surface displacements with sub-centimeter accuracy by exploiting large datasets of SAR images acquired over more than 20 years; affordable costs for monitoring large areas.

As a result the scientific community analyzed a number of case studies which successfully investigated potential and limits of the DInSAR techniques (for instance a comprehensive overview of applications to slow-moving landslides was recently provided by Wasowski and Bovenga, 2014). For what concerns the categorization of the data based on the spatial resolution, it is important to remark since now that in this work we refer to the GMES data warehouse specification (Brefort, 2011) where sensors with spatial resolutions higher than 4 m are classified as very high resolution (VHR) systems, whereas data with spatial resolutions in the range 4-30 m are referred to high resolution. In many publications it is, however, possible to find these two categories referred to as high and medium resolution, respectively.

As for natural or anthropogenic subsidence the available studies – carried out by using data acquired via European Space Agency (ESA) and Canadian Space Agency (CSA) high resolution (Brefort, 2011) ERS-1/2, ENVISAT SAR and RADARSAT-1/2 sensors – demonstrated the capability of DInSAR technology to monitor ground surface displacements induced by either mining (Carnec et al., 1995; Haynes, 2000; Kircher et al., 2003; Raucoles et al., 2003; Crosetto et al., 2005; Wang et al., 2009; Herrera et al., 2010a) or water extraction (Haynes, 2000; Galloway et

al., 2000; Cascini et al., 2006; Herrera et al., 2009b; Calderhead et al., 2011; Cigna et al., 2012; Sanabria et al., 2014; Tomás et al., 2014) or underground construction works (Giannico et al., 2012).

Recently, a breakthrough for the monitoring of subsiding urban areas at detailed scale ($> 1:5,000$) was provided by the last generation X-Band very high resolution (Brefort, 2011) SAR sensors TerraSAR-X/TanDEM-X (TSX/TDX) mission of the German Aerospace Center (DLR) and the Cosmo-SkyMed (CSK) constellation of the Italian Space Agency (ASI) (Herrera et al., 2010b; Cascini et al., 2013; Fornaro et al., 2014). Such sensors are characterized by a higher revisiting time than that pertaining to the ESA sensors (35 days); in particular, in the case of CSK the use of a constellation of satellites allows bringing the revisiting time down to 4 days (on average) thus providing exceptional capability of collecting stacks of data useful for interferometric analysis (about 30 SAR images) in a shorter time interval, i.e. few months instead of few years. Furthermore, the resolution improvement allows more details of single facilities to be observed and hence their precise monitoring, as testified by the available literature reporting on the use of TerraSAR-X data (Gernhardt et al., 2010; Zhu and Bamler, 2010; Reale et al., 2011a; Fornaro et al., 2012; Fornaro et al., 2013). Moreover, the recently launched (April 2014) Sentinel mission of the European Space Agency will provide continuity of ERS-1/2 and ENVISAT data archives with reduced revisiting times and large coverage swath.

Thanks to the reliability of DInSAR data, a number of international (TERRAFIRMA, 2013; Del Ventisette et al., 2013), national and regional (Meisina et al., 2008; Terranova et al., 2009; Risknat Project, 2012) projects all over the world were developed in the last years so that the end-users are currently provided with extensive datasets. An example in Italy is the “Piano Straordinario di Telerilevamento Ambientale – PST Project” (MATTM, 2010) offering a nation-wide coverage of high resolution SAR sensors from 1992 to 2010.

In spite of the applications and the future improvements offered by new satellites, standardized procedures allowing the reliable use of DInSAR data and their interpretation at all scales of analysis (i.e. small, medium, large and detailed according to Fell et al., 2008) are still lacking. To this aim, the present work wants to provide a contribution by first introducing a general framework to be followed when using DInSAR data to study natural or anthropogenic phenomena. Then, original procedures for the analysis of DInSAR data – deriving from different sensors or algorithms – are proposed with particular reference to the investigation of subsidence-induced ground displacements in urban areas. The proposed procedures are tested in well-documented sample areas of the Campania region (southern Italy) at four scales of analysis (small, medium, large and detailed according to Fell et al., 2008) by using DInSAR data resulting from the rich archive dataset of the Italian PST Project as well as from an available dataset of CSK data.

2 SAR sensors and DInSAR techniques

2.1 SAR sensors

The basic concepts and the first experimental demonstration of interferometric techniques were presented by Zebker and Goldstein (1986) for topographic mapping purposes and by Gabriel et al. (1989) for the detection and mapping of small elevation changes by using SEASAT SAR sensor operating in the period June-October 1978. However, the beginning of the development that brought interferometry to operational applications is associated with the launch of ERS-1 satellite in 1991, followed by the twin sensor ERS-2 launched in 1995. Starting from these sensors and boosted by evidence of the potential for applications of interferometric techniques, several other sensors were launched in the following years with a significant growth since 2007; many others are planned in the early next years. Figure 1 provides a picture of the historical evolution of the availability of SAR sensors since 1992 when ERS-1 became operative. The sensor working frequency are

generally allocated in the L, C and X bands, corresponding to wavelengths of about 18 cm, 5.6 cm and 3.1 cm, respectively.

SAR satellites are placed in the so called Lower Earth Orbits (LEO), between 500 km and 800 km, and follow polar orbits in order to provide a global coverage. Accordingly, scenes may be observed by SAR sensors over ascending or descending orbits typically with opposite ground looking directions.

Earlier SAR sensors were characterized by fixed swaths (i.e. fixed illumination beam width); modern sensors offer different operative modes (e.g. fine, strip, spot, scan) which allow a tradeoff between spatial coverage and spatial resolution. In other words, it is possible to have higher resolutions (e.g. up 1 meter for civil applications) with limited coverage (e.g. 10 kilometers) and coarser resolutions (e.g. 10 m) with wider coverage (e.g. a hundred of kilometers or even more).

Furthermore past generation SAR sensors were characterized by a fixed illumination direction, commonly referred to as Line Of Sight (LOS), whereas modern sensors allow the LOS to be conveniently set. For instance, the LOS angle with respect to the vertical direction was 23° for ERS-1/2 whereas for most of the currently operational sensors can range from 20° up to 50° . This ability to vary the illumination angle is important when imaging mountainous areas. Moreover, the possibility to change the LOS is also important for monitoring purposes because displacements measured by DInSAR techniques are components of the 3D ground displacement.

Taking into account that SAR satellite orbits are polar and radars image the scene typically in the broadside direction – which is orthogonal to the orbit direction – the LOS is almost belonging to the east-west/vertical plane. In particular, LOS direction is downward and being SAR sensors generally right looking, the LOS direction is eastward in ascending passes and westward in descending passes. Ground displacements occurring along North and South directions are, therefore, almost undetectable unless Multiple Aperture Techniques (MAI) – exhibiting significantly coarser

resolutions – are used (Jung et al., 2011). For instance, the so-called sensitivity unit vector (Massonet and Feigl, 1998; Colesanti et al., 2003) has components that for ERS/ ENVISAT sensors (in absolute values) are: 0.38 for the east component, 0.08 for the north component and 0.92 for the vertical component. Depending on the sub-swath, for recent satellites the east and the vertical component can be traded off whereas typical orbital inclinations do not allow changing significantly the north component sensitivity.

The time taken for a satellite to repeat the same orbit is called the ‘revisiting time’ (RT in Fig. 1); it determines the highest possible temporal sampling rate of signal (time series) associated with the measured target displacement. Depending on the orbit height as well as on the number of sensors for each satellite constellations the revisiting time ranges between tens of days to a day (Fig. 1).

Another key issue is that SAR sensors are coherent systems but the implementation of interferometric techniques, which are intrinsically characterized by a diversity factor of angular or temporal origin, requires that the scattering on the scene is coherent as well, and similarly that the scattering properties must not change ‘significantly’ over time. In the SAR jargon it is required that the measured echoes from the scene scattering centers are coherent (Fornaro and Pascazio, 2014). The coherence, which is routinely estimated on the available interferometric SAR dataset, can be quantified in terms of statistical characterization of the radar echoes: it is a number between 0 and 1; lower coherence means a higher interferometric phase noise contribution and vice versa. Vegetated areas are prone to temporal coherence losses whereas arid and built up areas are typically associated with higher coherence values, i.e. a better quality of the interferometric signal. The wavelength impacts the coherence; generally the larger the wavelength the higher the coherence. Therefore lower frequencies are more suitable for the observation of vegetated areas (Fornaro and Pascazio, 2014).

2.2 *DInSAR techniques*

Since early 2000s several multi-pass DInSAR algorithms have been developed and widely used to retrieve information on displacements of the topographic surface, among them: the Persistent Scatterers (PSInSAR) technique (Ferretti et al., 2000; Ferretti et al., 2001), the Small Baseline Subset (SBAS) technique (Berardino et al., 2002), the Coherent Point Target Analysis (CPTA) (Mora et al., 2003), the Stable Point Network (SPN) (Arnaud et al., 2003), the Interferometric Point Target Analysis (IPTA) (Wegmüller et al., 2005), the Spatio-Temporal Unwrapping Network (STUN) (Kampes and Adam, 2005), the Stanford Method for Persistent Scatterers (StaMPS) (Hooper et al., 2004) and the Enhanced Spatial Differences (ESD) (Fornaro et al., 2007). The available techniques for the analysis of phase signals in interferometric stacks can be grouped in two classes: Persistent Scatterers Interferometry (PSI) (Ferretti et al., 2000; Ferretti et al., 2001; Costantini et al., 2008; Crosetto et al., 2008) and Small-Baseline techniques (Berardino et al., 2002; Fornaro et al., 2009).

PSI techniques operate at full spatial resolution and identify reliable scatterers by measuring their multitemporal coherence related to the phase stability; monitored scatterers correspond to man-made structures (buildings, roads, bridges) or bare rocks whose size is smaller compared to the system resolution.

Conversely, the SBAS techniques are tailored to decorrelating scatterers (i.e. scatterers that may be distributed in the resolution cell or characterized by slow temporal change of the scattering) and to measure ground deformations over large areas (Berardino et al., 2002). These techniques take benefit of a spatial averaging (multilook) to improve the quality of the phase signal thus performing a change of the scale of analysis. Moreover, the interferograms are generated according to small temporal and spatial separation constraints in order to further reduce decorrelation effects associated with possible coherence losses typically present in the analysis of rural areas. The SQueeSAR

algorithm (Fumagalli et al., 2011) has been recently developed to perform a mixed scale of analysis which includes in PSInSAR processing the multilook operation and a data dependent weighting of interferograms in order to improve the capabilities of the original algorithm in the monitoring of decorrelating scatterers.

SBAS techniques are suitable for investigating ground deformations at medium scale but can be useful also to calibrate data for full resolution analysis. At the medium scale, the technique exploits averaged (multi-look) interferograms and allows the generation of mean velocity maps and associated time series for areas extending for some thousands of square kilometres (up to $100 \text{ km} \times 100 \text{ km}$), with a ground resolution typically of the order of $80 \times 80 \text{ m}$ (ERS-1/2 and ENVISAT). SBAS can be used also at large scale by exploiting single-look interferograms, i.e. generated at full spatial resolution (typically of the order of $10 \times 10 \text{ m}$ for ERS-1/2 and ENVISAT; $3 \text{ m} \times 3 \text{ m}$ for very high resolution sensors) (Lanari et al., 2004b); however the limitations on the baseline can lead to detection and localization accuracy loss with respect to PSI when dealing with persistent scatterers (PS) typically associated with man-made targets.

With reference to full resolution multitemporal DInSAR analysis, particularly suited for investigating single structures with high resolution sensors (Schack and Soergel, 2014), a recent advancement is represented by the introduction of tomography approaches (Fornaro et al., 2005) and, more specifically, the Multi-Dimensional Imaging technique (MDI) (Lombardini, 2005; Fornaro et al., 2009) which allows the identification, localization and monitoring of scatterers at full resolution with improved performances with respect to classical PSI approaches. MDI techniques fostered single building monitoring by retrieving better detection and estimation accuracy with respect to PSI also allowing the layover effects on vertical structures (e.g. buildings) – particularly evident in VHR systems – to be solved. MDI is currently used at an operational level by the German Aerospace Center (DLR) for the analysis of urban areas (Zhu, 2011; Wang et al., 2012)

with TerraSAR-X data. Furthermore, the resolution improvement allows the capture of more details of single facilities under observation and hence their precise monitoring, as testified by the available literature mainly focused on the use of TerraSAR-X data (Gernhardt et al., 2010; Zhu and Bamler, 2010; Reale et al., 2011a, 2011b; Fornaro et al., 2012; Fornaro et al., 2013).

A last comment is dedicated to the achievable accuracy of the DInSAR data which depends on a number of factors such as the wavelength, the coherence, the number of images, the overall temporal span and, last but not least, the confidence level of the processing algorithm and implementation issues which may depend also on the processed dataset. Quantitative assessments carried out by comparisons with independent measurements, such as in Colesanti (2003), Casu et al. (2006) and Herrera et al. (2009a), indicate that, as a rule of thumb, the accuracy is of 1-2 mm/year for the average displacement velocity and of 5-10 mm for the single time series displacement. An experimental evidence of the possibility to achieve an accuracy up to the order of 1 mm on a single displacement measurement was provided in Fornaro et al. (2013), although the results refer to the monitoring of a specific structure (a reinforced concrete bridge).

3 The proposed approach

The definition of a methodological approach in problems where input data derive from innovative technologies represents a necessary activity in order to enhance a good **practice** and to promote their diffusion. Accordingly, the present section **first** introduces a general framework for the use of DInSAR data; then, focusing on the application to subsidence phenomena, it briefly outlines the state of the art and finally proposes original procedures allowing the pursuit of different objectives at different scales.

3.1 *General framework*

Owing to the complexity of DInSAR data, as described in Crosetto et al. (2005), the most advanced applications and the best results are usually achieved through a close cooperation between DInSAR specialists and people able to use DInSAR data in order to analyse the danger at hand. In this context DInSAR specialists can play a fundamental role in helping the end-users to be fully aware of limits and potentials of the techniques. These concepts inspire the general framework proposed in Figure 2 which summarizes the sequence of activities involving the experts of both radar image processing (specific activities are framed in red) and the danger (specific activities are framed in blue). In particular, the first stage includes the definition of the problem, namely: the type of the danger (e.g. subsidence, slow-moving landslides) to be analyzed; the extent of the area to be investigated and the description of its specific features which most directly influence the use of satellite data (i.e. vegetation cover, presence of urbanized area, topographical and historical information about any changes occurred in the area during the period of observation, etc.).

Once the problem is defined, it is necessary to arrange the analyses to be performed by identifying: the aim and the scale (e.g. Fell et al., 2008) of the analysis; the period of observation; the mapping units (Guzzetti, 2005) – e.g. grid cell for subsidence phenomena or terrain units for slow-moving landslides – on which to carry out the analysis in a GIS environment. After this, there is an “exit/problem redefinition” option since in some cases DInSAR techniques cannot respond (or just partially) to the end-user’s initial problem (e.g. if the expected displacement rate is too high, for instance some dm/yr). So a decision has to be taken whether DInSAR will be used or it would rather need to be associated with other techniques (e.g. optical images, ground based data, etc.). On the contrary, in the case that DInSAR analysis can proceed, with the contribution of both experts it is possible to select the image dataset according to the characteristics of the available sensors such as: band, orbital data, geometry of acquisition, data resolution, stacks of available images on the

study area, revisiting time and swath. In this regard, it is worth pointing out that together with the wavelengths the revisiting time directly impacts the maximum measurable displacement over the time; more specifically it bounds the maximum spatial variation of the displacement between two consecutive observations (i.e. the bound acts on the displacement spatial variations and not on the displacement of a single point because DInSAR techniques work by integrating temporal and spatial variation between coherent pixels over the time and the space). It is for this reason that displacements measured by DInSAR techniques are referred to the known displacement of a single point, commonly referred to as reference point or tie point, generally assumed as stable point. Moreover, also the band influences the sensor selection since lower frequency bands (L band, i.e. longer wavelength sensors) are more suitable for the monitoring of faster dynamics, with the advantage, as previously pointed out, of penetrating the vegetation coverage; whereas higher frequencies (X band) provide a higher sensibility of the sensors to smaller displacements such as those due to thermal variation of the built up environment. A good compromise is provided by C band.

Once SAR images are chosen they undergo the processing phase via specific algorithms whose selection is in charge of both experts depending on the available input data and the expected outputs to be used in the analysis (e.g. velocity, time series, coherence, reference point).

The final step concerns the analysis of DInSAR data which, as it is shown in next sections for subsidence phenomena, can be carried out at different scales pursuing different aims.

3.2 *State of the art of the applications to subsidence phenomena*

The number of applications of DInSAR techniques to detect and monitor subsiding areas at different scales rapidly increased during the last decade. Table 1 lists some case studies available in

the scientific literature grouped according to the scale of analysis in turn related to the extension of the typical area to be zoned as suggested by Fell et al. (2008) (see also Section 3.3) .

For instance, with reference to the Piedmont region (northern Italy), Meisina et al. (2008) developed at small scale ($< 1:100,000$) a methodological approach for the interpretation of PSInSAR data via the preliminary detection of the so called “anomalous areas” wherein significant movements are recorded (clusters with a minimum of 3 PS having a maximum mutual distance of 50 m and displacement rates exceeding ± 2 mm/year); then, the interpretation is first carried out via the overlap, in a GIS environment, of anomalous areas with other layers (i.e. topographic map, geological map, orthophoto) that might have relevance in explaining the patterns of motions of PS points. At small scale, Vilardo et al. (2009) discriminated the vertical and east–west displacement components in Campania region (southern Italy) thanks to the availability of datasets referring to both ascending and descending orbits of ERS-1 and ERS-2 satellites. At medium scale (1:100,000 to 1:25,000), Cascini et al. (2007a, 2013) preliminarily detected the most critical zones of the Campanian Plain where the highest ground surface settlements occur, in terms of both magnitude and rate. At large scale (1:25,000 to 1:5,000), Herrera et al. (2009b, 2010b) used DInSAR data to successfully detect and monitor a recent subsidence affecting Murcia City (Spain) via the exploitation and the comparison of both C- and X-band satellite radars. Cascini et al. (2007b, 2011a, 2011b) proposed, at large scale, the map of settlements and the settlement gradient map, while at detailed scale ($> 1:5,000$) they derived relevant parameters widely adopted in engineering practice to assess building damageability. Based on this approach Sanabria et al. (2014) generated subsidence activity maps via a geostatistical analysis of DInSAR data, assessing buildings’ serviceability limit states at large scale. Arangio et al. (2013) integrated at detailed scale the results of DInSAR analysis with an intermediate semi-empirical model to investigate three buildings located in the southern part of the city of Rome. The model, originally proposed by Finno et al.

(2005), considers each building as an equivalent laminated beam where the layers represent the floors and the core material reproduces the infill walls. The results obtained by the model have been compared with the damages observed on the buildings, showing a good agreement.

In conclusion the analysis of the scientific literature highlights the availability of several interesting case studies, mainly carried out at a single scale of analysis. The following section shows the possibility of analyzing subsidence phenomena by a multiscale approach which is described by introducing a general framework useful for its generalization.

3.3 Proposed procedures for DInSAR analyses to be carried out at different scales in subsiding urban areas

The application of the general framework (section 3.1) to natural or anthropogenic subsidence phenomena at different scales calls for the definition of a set of procedures which are briefly outlined in this section and, then, applied to well documented case studies in section 4.

As it is shown in Table 2 different objectives can be pursued at different scales of analysis, ranging from small ($< 1:100,000$) to detailed ($> 1:5,000$). The analyses can be carried out either following a cascade multiscale approach (e.g. from the small scale to the detailed one) or focusing on a given scale.

As for the mapping units, a grid dividing the territory into regular areas (“cells”) of pre-defined size (e.g. Carrara, 1983; van Westen, 1993; Guzzetti, 2005) is proposed; in this regard the analyses presented in this work assume the side of each cell as coinciding with a fraction (e.g. $1/1,000$) of the scale dimension.

Another key point is the selection of the most appropriate SAR dataset which mainly results from a compromise among three different factors: the period of observation required for the analysis at hand (i.e. this issue influences the selection because of the availability of a given archive); the scale

of the analysis; the cost-effectiveness of the analysis. Referring to the latter two points it has been proven that both high and very high resolution SAR sensors (Fig. 1) can be used for analyses at different scales – being very high resolution ones preferable for detailed analyses – provided that the level of details balance the amount of data and affordable costs.

As for the objectives to be pursued at different scales, the main goal of the analysis at small scale ($< 1:100,000$) is to detect moving portions of large areas in order to inform policy makers and dwellers. This kind of analyses poses the problem of managing massive DInSAR datasets over large areas independently of the selected sensor. If a cascade approach is followed the results obtained at small scale can address the analyses at medium scale ($1:100,000$ to $1:25,000$) just within the areas zoned as moving. At this scale, the aim of the analysis is to draw the inventory of the affected municipalities as well as their ranking. This information can be exploited in land use planning and management activities such as the evaluation of possible constraints in the development of large engineering projects (Fell et al., 2008). As far as the analysis at large scale ($1:25,000$ to $1:5,000$) is concerned, the main aim is to zone the built up areas within the most affected municipal territory where damage occurred or is likely to occur; moreover, a preliminary analysis of damage severity can be carried out in order to plan suitable zones for urbanization expansion or to detect damaged/likely damaged urbanized areas. Finally, the analysis at detailed scale ($> 1:5,000$) can provide a close look into the behaviour of single buildings experiencing subsidence-induced settlements, also making possible the application of commonly used damageability criteria (e.g. Skempton and MacDonald, 1956; Burland and Wroth, 1974) for both back-analysis and forecasting purposes provided that a proper DInSAR data coverage is available.

3.3.1 Small scale

For the purposes of small scale analyses the extension of the typical area of zoning is higher than $10,000 \text{ km}^2$ (Fell et al., 2008); the adopted grid of analysis can have a cell size larger than of 100 m

×100 m (Table 2). As it is shown in Figure 3 the proposed approach at small scale consists of four working phases plus a preliminary one; the input data (derived at a given phase from the output of the previous phases and/or external data), the procedure and the output – this latter generally furnished as maps – are also reported for each phase of the analysis.

The preliminary phase is preparatory for the operative grid of analysis as well as for DInSAR data mapping; in this phase the input data are the Digital Terrain Model (DTM) and the DInSAR data. In particular, the operative grid of analysis is set on flat areas (e.g. with slope angles not exceeding 3° according to Trigila and Iadanza, 2007), in turn extracted from the slope angle map (derived by the DTM), where the analyses will be focused. Then, DInSAR data are treated to take into account the localization error (e.g. by drawing in a GIS environment an operative buffer around the point-wise DInSAR information on the ground).

In phase I_(s) the aim is to detect DInSAR covered cells. In particular, each cell is defined as covered if at least one PS/coherent pixel falls within its perimeter. As a result, cells covered by DInSAR data acquired on ascending orbit, descending orbit and by their combined information are distinguished.

The aim pursued in phase II_(s) is the detection of moving areas. With reference to DInSAR data acquired on ascending and descending orbit, the average DInSAR velocity value is computed for each covered cell according to the Equation:

$$vel_{a,C} = \frac{\sum_{i=1}^N w_{ci} V_i}{\sum_{i=1}^N w_{ci}} = \sum_{i=1}^I \frac{w_{ci}}{w_{cN}} V_i, \quad w_{ci} = \frac{(1 - \epsilon_{min})}{(C_{max} - C_{min})} (C_i - C_{min}) + \epsilon_{min} \quad (1)$$

which allows the computation of the average velocity modulus along the LOS direction by weighting PS LOS velocity values on their coherence values.

In the Equation (1): i refers to the i^{th} PS within the grid cell; N is the total number of PS within the grid cell; w_{ci} is the weight computed on coherence of the velocity of the i^{th} PS within the grid cell; w_{cN} is the sum of w_{ci} ; V_i is the velocity of i^{th} PS; C_{\max} is the maximum coherence value of the used dataset; C_{\min} is the minimum coherence value of the used dataset; C_i is the coherence value of the i^{th} PS within the grid cell; ε_{\min} is a given very small number used in order to not discard the i^{th} PS with $C_i = C_{\min}$.

Thus operating the analyses take into account the coherence values which, although defined in different ways by the available algorithms, can be considered as a reliability parameter to be associated with each PS velocity/displacement value (Cascini et al., 2013).

Once the weighted average LOS velocity value for each grid cell is computed, a velocity threshold varying according to the sensor used and the temporal sampling (e.g. for C-band sensors it can be assumed equal to 1.5 mm/year according to Cascini et al., 2010; for sensors operating at other bands suggestions are given by Bianchini et al., 2014 and Notti et al., 2014) is introduced, so allowing each cell to be appointed as moving (average velocity value exceeding the threshold), not moving (average velocity value lower than the threshold) and not covered (if no PS were found in the singular grid cell); the corresponding output is the map of moving areas.

Phase III_(s) addresses the computation of the Subsiding Plain Index (I_{SP}) (Eq. 2) as the ratio between the extension of the moving cells (C_m), the extension of the covered cells (C_c) and the extension of the cells within the i^{th} Plain (P_i) of the study area normalized to the same terms referring to the whole study area. Accordingly:

$$I_{SP} = \frac{\left(\frac{C_m}{C_c} \right)_{Pi}}{\sum_{Pi=1}^n \left(\frac{C_m}{C_c} \right)_{Pi}} \quad (2)$$

Phase IV_(s) pursues the definition of the prevailing moving direction recorded within the moving areas detected in phase II_(s). In particular, focusing on the moving areas, only those cells with data on both orbits are selected in order to apply a procedure for the ascending and descending data combination which allows extracting the vertical (z) and east-west (EW) velocities. To this aim, by referring to Cascini et al. (2010), where it is outlined a general procedure for the projection of the measured ascending and descending velocity components (V_{LOS_A} and V_{LOS_D} respectively) along a direction selected according to a model suited to the specific application, it is possible to derive a simple relationship linking the V_{LOS_A} and V_{LOS_D} to the vertical and horizontal velocity components (V_z and V_E , respectively) (see also Manzo et al., 2006). Accordingly, with reference to Cascini et al. (2010, 2013) and the mathematical formalism therein adopted, by assuming the orbits along the South-North direction (i.e., $r_{AE} = -r_{DE}$, $r_{AZ} = -r_{DZ}$), and by neglecting hence the NS velocity component of the displacement $r_{AN} = r_{DN} = 0$, i.e. by letting $u_N = 0$, the EW and vertical velocity components can be simply derived as:

$$v_z = (v_{LOS_A} + v_{LOS_D}) / (2r_{AZ}) \quad v_E = (v_{LOS_A} - v_{LOS_D}) / (2r_{AE}) \quad (3)$$

wherein, the relationships between the ascending and descending LOS unit vector components $r_{AE} = -r_{DE} = \sin(\alpha)$ and $r_{AZ} = r_{DZ} = \cos(\alpha)$ with α being the incidence angle, have been exploited for the derivation of Equation (3).

As Cascini et al. (2013) proposed, once considered the ratio between horizontal and vertical velocity modulus ($|V_E/V_Z|$) in each cell, the prevailing movement can be assumed as horizontal for ratio values greater than 1.73 (corresponding to the value of the tangent of an angle of 60° between the movement direction and the vertical axis), horizontal/vertical for ratio values between 1.73 and 0.57 (corresponding to the value of the tangent of an angle of 30° between the movement direction and the vertical axis) and vertical for ratio values lower than 0.57. The output of the analysis performed in phase IV_(s) is called the “advanced map of moving areas” which can be more easily exploited for the interpretation of the phenomena (see, for instance, Vilardo et al., 2009).

3.3.2 Medium scale

The main goal of the analysis at medium scale is the inventory of the affected municipal territories and their relative ranking. The analysis can take advantage of the results obtained at small scale (e.g. map of moving areas represented with a dotted frame in Fig. 4) or they can be carried out independently on a given area of interest. The typical area of zoning is between 1,000 and 10,000 km² (Fell et al. (2008)); the operative grid varies from 25 m × 25 m to 100 m × 100 m (Table 2). The flow-chart of Figure 4 shows the steps to be carried out which can be divided in two working phases besides a preliminary one. During the preliminary phase the operative grid of analysis is set on the moving areas detected at small scale.

Since the activities of phase I_(m) pursue the detection of moving urbanized area, the cells covered by ascending and descending data are first selected and, for each of them, weighted velocity values are computed (Eq. 1). Then, the velocity threshold (see section 3.3.1) is introduced, thus allowing each cell to be appointed as moving, not moving and not covered. The corresponding output is the map of the moving areas which, in turn, is intersected with the map of the urbanized area in order to derive the map of the urbanised area with evidence of movement. This latter output can be used in

phase $\Pi_{(m)}$ to map the subsiding municipalities and to rank them according to the so-called Subsiding Municipality Index (I_{sm}) defined as:

$$I_{sm} = \frac{\left(\frac{U_m}{U_c} \right)_{M_i}}{\sum_{M_i=1}^n \left(\frac{U_m}{U_c} \right)_{M_i}} \quad (4)$$

wherein U_m is the extension of the urbanized area with evidence of movement, U_c is the extension of the covered urbanized area, U_{tot} is the extension of the urbanized area, M_i refers to the i^{th} Municipality within the considered test area.

Accordingly, the highest values are associated with the most affected municipalities in which more detailed analyses are first required.

3.3.3 Large scale

The aim of the analysis at large scale is to zone built up areas where damage to facilities occurred or is likely to occur. The analysis can focus on the territory of the municipalities which resulted as subsiding from the analysis at medium scale (e.g. map of subsiding municipalities represented with a dotted frame in Fig. 5) or they can be carried out independently on a given municipality. The typical extension of the area of zoning, according to Fell et al. (2008), is between 10 and 1,000 km²; the operative grid ranges from 5 m × 5 m to 25 m × 25 m (Table 2).

As it is shown in Figure 5 an operative grid is set in the preliminary phase. Then (phase $I_{(1)}$), the map of east-west/vertical velocity is derived with the procedure described in section 3.3.1. Subsequently the map of cumulative displacement components is derived by multiplying the

average east-west/vertical velocity by the time of observation. In phase II₍₁₎ the analyses are focused only on the areas in which the prevailing direction is vertical (i.e. map of settlements). Accordingly, the outputs of phase II₍₁₎ is the map of settlement gradients with their prevailing directions. These results allow the area where damage occurred, or is likely to occur, to be zoned within the municipal territory by assuming, for instance, some threshold values relevant to typical parameters adopted in damageability criteria (Cascini et al., 2011a).

3.3.4 Detailed scale

Detailed scale studies are suitable for the analysis of single structures where damage is likely to occur/to be occurred as a result of either large scale analyses (i.e. map of settlement gradients with their prevailing directions represented with a dotted frame in Fig. 6) or information gathered from field surveys (Fig. 6). In the former case, detailed scale analyses can be carried out by prioritising DInSAR covered buildings which at large scale exhibit the highest values of relevant parameters, such as settlement gradients; otherwise, it can be extended to all subsidence-affected buildings (preliminary phase). It is worth stressing that the reliability of the results achieved at this scale of analysis is influenced by the coverage and, particularly, by the distribution of DInSAR data on the target. In order to tackle this key point, an original procedure for the selection of those buildings best fitting the analysis is proposed. In particular, for each building the Coverage Index is computed:

$$I_{\text{coverage}} = \frac{A_c}{A_{\text{tot}}} \times 100 \quad (5)$$

where: A_c is the area of the portion of the building which is covered by DInSAR information; A_{tot} is the area of the building. This Index is obviously dependent on the resolution of the used sensor.

In phase I_(d), referring to the selected building/buildings east-west/vertical velocities (Eq. 3) are computed for each grid cell covered by both ascending and descending orbits. Then, the displacement components are derived (see section 3.3.3) and in phase II_(d) multi-temporal profiles of displacement components along fixed sections as well as of other settlement-derived parameters, such as relative rotations (Burland and Wroth, 1974), are computed in order to apply damageability criteria. It is worth stressing that sections of analyses can be selected either according to the prevailing directions of settlement gradients derived at large scale or on expert knowledge basis.

For sake of completeness, the scientific literature on the topic offers a variety of damageability criteria which can be grouped in three main categories: empirical methods (e.g. Skempton and MacDonald, 1956; Polshin and Tokar, 1957; Bjerrum, 1963); methods using structural engineering principles (e.g. Burland and Wroth, 1974; Boscardin and Cording, 1989; Finno et al., 2005); methods based on numerical modelling (e.g. Burd et al., 2000). For the purpose of the present study it is worth stressing that passing from empirical methods to numerical modelling requires more and more detailed information with reference to both components (horizontal and vertical) of displacements concurring to the buildings' damage occurrence.

4 Results

The test area selected for the analysis at small scale is the Campania region (southern Italy) which includes the southern Apennines chain and Plio-Quaternary structural depressions over an area of about 13,600 km². The analysis at medium scale concerned the Campanian Plain which is the largest coastal plain along the Tyrrhenian Coast in central-southern Italy, extending for about 2,000 km²; with reference to Baronissi municipality (included in the Campanian Plain) large scale analyses were carried out. Finally detailed analyses dealt with two buildings located respectively in Baronissi and in the suburbs of Naples city.

The DInSAR dataset used for the analyses derives from the processing of both high and very high resolution SAR sensor images (see Tables A.1-3 in the Appendix). In particular, the DInSAR measurements from high resolution ERS-1/2 and ENVISAT satellites were collected within the Italian ‘Piano Straordinario di Telerilevamento Ambientale’ (MATTM, 2010), which provides the results of the processing data acquired by those sensors via PSI techniques. The data archive spans a wide temporal interval from 1992 to 2010 and includes results of the processing of data acquired on ascending and descending orbits of the satellites. In Table A.1, the list of the different interferometric datasets exploited for the analysis, the corresponding PST cluster reference as well as the scale of analysis they were used for are reported. Data provided by the PODIS_Tellus regional project (Terranova et al., 2009), resulting from the processing of RADARSAT-1 sensor (Table A.2), were also exploited. The time interval spanned by these acquisition is shorter with respect to the former ERS and ENVISAT archives and is limited from 2003 to 2007. Finally, for the analysis at a detailed scale, data acquired by the COSMO-SkyMed constellation on descending orbits in the standard HIMAGE stripmap mode, characterized by a spatial ground resolution of 3 m \times 3 m with an average incidence angle of about 35°, were also exploited. In this case, the data were directly processed via SAR Tomography (Fornaro et al., 2009) to retrieve ground velocity measurements. Respect to the former ERS, ENVISAT and RADARSAT satellites, the dataset is composed by a smaller number of images (28), acquired on ascending orbit in only one year, from February 2010 to February 2011 (Table A.3).

4.1 Analyses at small scale

Campania region (Figs. 7a-d) has a complex geological structure, characterized by the interplay of several geodynamic processes related to the presence of active volcanoes (Vesuvius, Phlegraean Fields and Ischia), widespread landslide and subsidence prone-areas as well as from long to short

term tectonic warping which produce ground deformation pattern (Milone and Scepi, 2011; Vilardo et al., 2009). These factors make the studied region particularly complex.

At small scale the aim of the analysis is the detection of areas affected by subsidence-induced displacements (see section 3.3.1). For this purpose the dataset of the Italian ‘Piano Straordinario di Telerilevamento’ (MATTM, 2010) were exploited for the Province of Avellino, Benevento, Caserta; moreover, ERS-1/2 and RADARSAT-1 datasets – provided by the PODIS_Tellus regional project (Terranova et al., 2009) – were used for Salerno Province.

Following the flowchart shown in Figure 3, the analysis at small scale focused only on flat areas derived from the DTM (Figs. 7a and 7c) by filtering out those areas with a slope angle (Fig. 7b) exceeding 3° according to Trigila and Iadanza (2007).

Then, an operational grid (Fig. 7d) with a spacing of $250\text{ m} \times 250\text{ m}$ was set. PS point-wise data derived on both orbits from ERS-1/2, ENVISAT and RADARSAT-1 sensors were then buffered with a circle of 10 meter diameter in GIS environment in order to tackle the positioning error (Colesanti and Wasowski, 2006).

In the phase $I_{(s)}$ (Fig. 3) the cell covered by DInSAR data – for each sensor and acquired on either ascending or descending orbit or on both of them – were selected. Accordingly, over a total of 105,286 cells covering the flat areas of Campania region: 46,696 (44 %) are covered by ERS-1/2 ascending; 43,833 (42%) by ERS-1/2 descending while 55,212 (52%) by ERS-1/2 ascending or descending; 55,717 (53%) are covered by ENVISAT ascending; 46,833 (44%) by ENVISAT descending while 58% by ENVISAT ascending or descending. Referring to Salerno Province over a total of 30,457 cells: 14,830 (48%) are covered by RADARSAT-1 ascending; 14,983 (49%) by RADARSAT-1 descending while 17,070 (56%) by RADARSAT-1 ascending and descending.

Thus operating within each selected grid cell and referring separately to ERS-1/2, ENVISAT and RADARSAT-1 on both orbits, in the phase $II_{(s)}$ (Fig. 3) the average velocity modulus along the

LOS direction was computed according to Equation 1. Subsequently, a movement threshold equal to 1.5 mm/year (Cascini et al., 2010) was introduced as described in section 3.3.1. The retrieved moving cells merged in single maps for each sensor in order to derive the so-called moving areas are shown in red in Figures 8a-c. The moving areas over the whole period were finally derived by considering the moving cells in common to either ERS-1/2 and ENVISAT data (for Avellino, Benevento and Caserta Provinces) or and ERS-1/2 and RADARSAT-1 data (for Salerno Province) (Fig. 8d).

The analysis of the obtained maps reveals that, despite a lack of information in rural areas, a percentage of Campania region territory, ranging from 19% up to 25%, is affected by ground displacements according to ERS-1/2 and ENVISAT data respectively.

Then, over the whole period of observation (about 20 years), the cells appointed as moving are 4,283, corresponding to 9% of those covered by ERS-1/2, ENVISAT and RADARSAT-1 datasets (Fig. 8d). These cells clearly concentrate on the most important plains of Campania region, namely: the Campanian Plain, the Sele Plain and the Valdiano Plain (Fig. 8d).

In the phase III_(s) the ranking of the plains of Campania region affected by subsidence was carried out by computing the Subsiding Plain Index (I_{SP}) (Eq. 2) The results (Fig. 9) highlight that the most affected area is the Campanian Plain whose I_{SP} reaches 81%. As it will be shown in the next section the obtained results found their confirmation in several previous studies.

Finally, in the last step (phase IV_(s)), the advanced map of subsiding areas was generated (Fig. 10). In particular, focusing on the moving cells detected in Figure 8 for each sensor, only those cells with data on both orbits were selected in order to apply the procedure for ascending and descending data combination (Manzo et al., 2006; Cascini et al., 2010) which allows the retrieval of the vertical (z) and east-west (EW) velocities. Consequently, according to the procedures described in section 3.3.1, the prevailing movements were obtained with reference to the flat areas of Campania region.

This analysis, for each SAR sensor, concerned – on the average – around 70% out of covered cells; among these, about 6% resulted as moving.

4.2 Analyses at medium scale

Owing to its rich environmental resources and its proximity to Naples town the whole territory of the Campanian Plain was highly exploited by intensive anthropogenic activities (e.g. groundwater withdrawals; huge urban development; etc.) since the end of the Second World War. As a result, several areas therein were affected by ground settlements of either natural or anthropogenic origins, as it is testified by a number of studies available in the scientific literature (Cascini et al., 2007a, 2013; Vilardo et al., 2009; ISPRA, 2012). The analysis at medium scale was carried out according to the procedure of Figure 4. Therefore, an operational grid with a spacing of $100\text{ m} \times 100\text{ m}$ was preliminary set on the study area. The analysis of phase $I_{(m)}$ was carried out similarly to Cascini et al. (2013) where the generation of the maps of urbanized area with evidence of movement is described in details. The main results functional to the present work are synthesized in Figure 11 with reference to three different periods: 1992-2001 (Fig. 11a); 2003-2010 (Fig. 11b) and 1992-2010 (Fig. 11c). In particular, Cascini et al. (2013) pointed out that via the superimposition of the moving/not moving cells according to ERS-1/2 data over the map of the urbanized area dated 2001 (derived from the ‘land-use map’ at 1:50,000 scale provided by Campania region) it was possible to derive that 88% of the urbanized area resulted covered by ERS-1/2 -PS cells and 43% out of the covered urbanized area resulted as moving over the period 1992-2001. Similarly, the intersection of the map of moving cells according to ENVISAT data with the map of urbanized area dated 2009 (derived from the ‘land-use map’ at 1:50,000 scale provided by Campania region) allowed the detection of the portions of urbanized area (covered for 89% of its total extension) which resulted as

moving (18%) during the period 2003-2010. Finally, Figure 11c shows that around 11% out of the covered urbanized areas exceed the moving threshold over the whole period 1992-2010.

Starting from the results obtained by Cascini et al. (2013) and according to the flowchart of Figure 4 the Phase II_(m) was developed (Figs. 12 a-c) in order to inventory and rank the affected municipalities according to the values of the Subsiding Municipality Index (I_{sm}). The analysis was carried out with reference to the same periods analyzed in Figures 11a-c. As for the period of observation coinciding with ERS-1/2 time series (1992-2000) the map of subsiding municipalities in Figure 12a highlights that, among the most affected ones ($I_{sm} > 5\%$), Castel Volturno (Caserta Province) and Naples can be mentioned. The former is discussed in the following, whereas the latter is addressed by Cascini et al. (2007a; 2013). As for the municipalities attaining $1\% < I_{sm} < 5\%$, previous studies (Cinque et al., 1987; Cascini et al. 2006, 2007a, 2007b, 2011a, 2011b) concerning Sarno (Salerno Province) demonstrated that the town (Figs. 13a-d) suffered from a subsidence phenomenon induced by huge groundwater withdrawals causing damage of different severity to both masonry (Fig. 13c) and reinforced concrete buildings (Fig. 13d).

Then, turning the attention to the map of the urbanized area dated 2009 with indication of evidence of movement for the period 2003-2010 (Fig. 12b) the most affected ones ($I_{sm} > 5\%$) resulted Castel Volturno, Naples, Pozzuoli and Torre del Greco. As for Pozzuoli (Naples Province), it includes the Phlegraean Fields area whose bradyseism and related effects are widely discussed by Lanari et al. (2004a); whereas Torre del Greco (Naples Province) falls within the ring-like zone bordering the Vesuvius volcano, dealt with in the scientific literature by Borgia et al. (2005). Amongst the municipalities attaining $1\% < I_{sm} < 5\%$, Baronissi (Salerno Province) is included. The result concerning Baronissi was validated by in-situ surveys recently carried out showing the occurrence of damages induced by settlements (see sections 4.3 and 4.4).

Finally, the map of subsiding municipalities (Fig. 12c) for the whole period of observation 1992-2010 – where subsidence phenomena of a prevailing natural origins and, thus, occurring for the whole period were expected to be detected – shows that amongst the most affected municipalities the well documented case of Castel Volturno is ranked. This further confirmation can be considered as a sort of preliminary validation of the developed analysis. Indeed, Castel Volturno area (Figs. 14a-b) is affected by both complex erosion processes affecting the whole coastline (Cocco et al., 1993) and widespread subsidence phenomena (Corniello et al., 2010). These latter, in turn, can be associated with huge groundwater withdrawals which also caused the sea ingression into land (salt-wedge) (Cascini et al., 2007a).

4.3 Analyses at large scale

Baronissi municipality (Fig. 15a) is located in Salerno Province in a flood plain, bordered by the carbonatic ridge of southern Apennines. The subsoil mainly includes alluvial deposits deriving from weathering processes affecting the rocks constituting the surrounding reliefs as well as from transportation phenomena of pyroclastic soils originated by the explosive activity of Phlegraean Fields and Somma-Vesuvius volcanic complexes (Santoro, 2001). In the study area 14 buildings were built in the period spanning from 2002 to 2003 (Figs. 15b-c). The buildings have basements used as garage, a colonnade at the ground floor devoted to commercial use and three or four floors for residential use. They have reinforced concrete frames with rectangular section columns and concrete slab; the foundations are of shallow type, in particular, grade beam or grade slab (Ascione et al., 2011).

As reported by the technical office of Baronissi starting from May 2011 damages to the buildings were recorded in the study area either affecting the functionality of underground garages or

compromising building aesthetics due to the opening of significant cracks at the joints between contiguous buildings.

According to the framework of Figure 5, after selecting the cell size of the operative grid (i.e. 10 m \times 10 m), in the phase I₍₁₎ the map of east-west and vertical displacement components can be generated. For the case study of Baronissi this map could not be derived by adopting a cell-based approach due to the small number of cells covered on both ascending and descending orbit. However, in order to gather this information useful for phase II₍₁₎ a qualitative analysis was carried out by interpolating via the Inverse Distance Weighting (IDW) method the available data (Cascini et al., 2011a). As it can be observed in Figures 16a and 16b in the study area during the period 1992-2000, velocity values exceeded – both in the horizontal direction and vertical direction – the movement threshold equal to 1.5 mm/year (Cascini et al., 2009) only in very limited portions of the territory. With reference to the period 2003-2007 (Figs. 16c-d), which, as above mentioned, coincides with the completion of the construction works of almost all of the buildings in the area, the average velocity recorded by PS data increased considerably, reaching values higher than 5 mm/year. It is worth stressing that DInSAR data interpolations, especially if framed within a quantitative analysis, should include estimations of the spatial variability and a confidence level on the interpolations as shown by Sanabria et al. (2014).

In order to investigate the relationship between the magnitude of settlements and the building damage occurrence, the analysis was then focused only on PS covered cells in the subsiding area. In particular, for each covered cell the average cumulative settlement – computed along its prevailing direction (vertical in this case) by multiplying the average vertical velocity by the time of observation and also weighting it on the coherence of PS data – was derived (Fig. 17a) using both RADARSAT-1 and ENVISAT data. This combined use allowed the improvement of data coverage in the area; in particular, both datasets were used to compute the cumulative settlements from 2003

to 2007 and, then, only ENVISAT data were used from 2007 to 2010 due to the lack of RADARSAT-1 data for this period.

Subsequently, since damage occurrence and severity in a given building can be related to the magnitude of settlement-derived parameters describing its foundation movements – like the so-called angular distortion or relative rotation (Skempton and MacDonald, 1956; Burland and Wroth, 1974) – a further step towards the analysis of consequences dealt with the generation of the map of settlement gradient vectors (Fig. 17b). These latter, whose direction coincides with the maximum rate of change of settlement, were computed in GIS environment on the cell grid starting from the measured cumulative settlements of Figure 17a. The obtained settlement gradient moduli were grouped into three classes (High, Medium, Low) according to their natural breaks distribution.

The results were then validated by in-situ surveys recently carried out (Figs. 17c-d) showing that, notwithstanding the limitation due to DInSAR data coverage, damage occurred where the highest settlement gradient moduli were reached as in the case of the two buildings framed in blue and in red in Figures 17a-b.

4.4 Analyses at detailed scale

The analysis via high resolution SAR sensor data was focused on one building (framed in blue in Figs. 17a-b) of Baronissi town which, as a result of the analysis at large scale, exhibited a high modulus of settlement gradient and one of the highest value of I_{coverage} (i.e. more than 30%). The structure consists of five reinforced concrete blocks structurally separated by 20 cm wide joints with rectangular section columns and concrete slab; the foundations are shallow grade beams. According to the structural report and the static testing of the building the construction works started in November 2002 and finished in March 2003 (Ascione et al., 2011).

According to Equation 1 the average velocity (Eq. 1) for each cell ($5 \text{ m} \times 5 \text{ m}$) covered by ENVISAT and/or RADARSAT data was first computed; then, since the results of Figure 16 revealed a prevailing vertical movement on the building cell average velocity values were projected along the vertical direction. Subsequently, by assuming a constant trend of the settlement time series relevant to both ENVISAT and RADARSAT-1 sensors the cumulative settlement for each covered cell of the grid was derived at different dates up to 2011 (Fig. 18a) considering that damages occurred in May 2011 (see section 4.3). After selecting the direction of the profile in agreement with the maximum settlement direction exhibited in Figure 17b, the trends of settlements with time were retrieved for four of the five blocks composing the building at hand (Fig. 18b) since the block labelled with letter E does not exhibit condition of movement (velocity values falling in the range $\pm 1.5 \text{ mm/year}$).

It can be observed that all blocks experienced an increase with time of their absolute settlements, being the block labelled with D the one reaching the maximum value (7.8 cm) (Fig. 18b). It is worth noting that an in-situ damage survey recently carried out in Baronissi revealed (Figs. 18c-d-e) that the block D recorded widespread cracks on the outside pavement and on infill walls as well as on the structural joints with the blocks C and E.

As already pointed out in section 3.3 very high resolution DInSAR data best fit analyses at detailed scale; accordingly, for sake of completeness a second example is shown in Figure 19a-g with reference to a row of two/three floored reinforced concrete buildings located in the suburbs of Naples city for which COSMO-SkyMed data were also available. Figures 19 a-b show the distribution of ERS-1/2 and ENVISAT data, respectively, and Figure 19c proves that the test structures (framed in yellow) fall at the boundaries between a group of moving and not moving cells ($100 \text{ m} \times 100 \text{ m}$, as result of the analysis at medium scale) over the whole period 1992–2010 according to ERS-1/2 and ENVISAT data. Figure 19d clearly shows the huge increase of COSMO-

SkyMed data coverage, although this latter dataset refers only to one orbit. By projecting the available velocity values along the vertical direction and, then, by assuming a constant velocity over time the averaged cumulative settlements were derived for each cell of the grid (5 m x 5 m) for the period of observation (Fig. 19e). Then, a longitudinal settlement profile was sketched in Figures 19e-f according to section 3.3.4 (Cascini et al., 2007b, 2011a, 2011b). The profile over the covered cells (it is discontinuous since some grid cells are not covered) shows that the first group of buildings (moving downward along the profile and eastward in the diagram) experiences settlements up to 1 cm in one year of observation; whereas the second group does not exceed 5 mm settlements. Further interesting information is gathered (Fig. 19f) by the trends exhibited by the angular distortion β – the rotation of the line joining two reference points on the foundation relative to the rigid body rotation of the whole superstructure – adopted by Skempton and MacDonald (1956) in their damageability criterion as a measure of the building distortion. This latter diagram highlights rather null values of β along the whole profile, thus implying the absence of damage in each single structure. An in situ damage survey recently carried out in the area revealed the presence of some vertical cracks just in correspondence of the structural joints between different structures (Fig. 19g). This evidence justifies the results of DInSAR analyses since the recorded damages could be related to relative settlements (slightly different in magnitude) of contiguous buildings rather than to differential settlements affecting the foundations of each single structure.

5. Concluding remarks

The present work introduced a general framework and scale-specific procedures tailored for the use of DInSAR data in the study of subsidence phenomena affecting urban areas. Thanks to a validation process based on in-situ observations the results of the analyses carried out with reference to well-documented case studies of the Campania region (southern Italy) showed the capability of the

proposed procedures to pursue goals commensurate with the scale of analysis (varying from small to detailed). Although this outcome encourages the straight adoption of the proposed scale-specific procedures, it is worth to observe that upcoming deepening on errors and inaccuracies will increase the robustness of the methodological approach as well as the reliability of the results. In this regard, a capillary field survey concerning the buildings in the subsiding areas under investigation will contribute to the fulfilment of the above aims as well as to the generation of fragility and vulnerability curves (Negulescu and Foerster, 2010; Saeidi et al., 2012) to be used for forecasting purposes.

Considering that subsidence phenomena at present affect many megacities all around the world with huge yearly economic loss and taking into account the lack of official Plans for subsidence risk management (e.g. in Italy), the procedures presented in this work together with the results achieved by the scientific community encourage further efforts towards the proposal of widely shared recommendations. These latter could allow the authorities in charge of land-use management and planning as well as the technicians to confidently use DInSAR data in the analysis at different scales of subsidence and related consequences to exposed facilities.

Appendix

Table A.1. List of the datasets from the PST project archive exploited for the analyses (S = small, M = medium, L = large, D = detailed).

Sensor	Orbit Direction	PST Cluster	Period of acquisition	nr. of images	SCALE			
					S	M	L	D
ERS	Ascending	PST_ERS_T129_F819_CL001_AVERSA	14/06/1992-13/12/2000	66	X	X		
		PST_ERS_T129_F819_CL002_CASSINO	27/06/1995-13/12/2000	53	X	X		
		PST_ERS_T129_F819_CL003_TEANO	14/06/1992-13/12/2000	66	X	X		
		PST_ERS_T129_F801_CL001_CAPRI	10/01/1993-13/12/2000	66	X	X		
		PST_ERS_T129_F801_CL002_SARNO	10/01/1993-	66	X	X	X	X

			13/12/2000					
		PST_ERS_T358_F819_CL001_BASELICE	08/09/1992-24/11/2000	47	X			
		PST_ERS_T358_F819_CL002_BENEVENTO	08/09/1992-24/11/2000	47	X			
		PST_ERS_T358_F819_CL003_CAPOSELE	08/09/1992-24/11/2000	47	X	X		
		PST_ERS_T358_F801_CL001_AQUARA	08/09/1992-24/11/2000	47	X			
		PST_ERS_T358_F801_CL002_CAMEROTA	08/09/1992-24/11/2000	47	X			
ERS	Descending	PST_ERS_T265_F2781_CL001_BENEVENTO	24/06/1992-23/12/2000	66	X	X		
		PST_ERS_T265_F2781_CL001_RICCIA	11/11/1992-23/12/2000	60	X			
		PST_ERS_T265_F2781_CL001_SALERNO	11/11/1992-23/12/2000	72	X	X	X	X
		PST_ERS_T36_F2763_CL001_CASSINO	08/06/1992-07/12/2000	72	X	X		
		PST_ERS_T36_F2781_CL001_CASERTA	08/06/1992-07/12/2000	76	X	X		
		PST_ERS_T36_F2781_CL001_NAPOLI	08/06/1992-07/12/2000	76	X	X		
		PST_ERS_T36_F2781_CL002_CAPRI	08/06/1992-07/12/2000	76	X			
		PST_ERS_T494_F2781_CL001_CERIGNOLA	10/07/1992-04/12/2000	78	X			
		PST_ERS_T494_F2781_CL001_EBOLI	10/07/1992-04/12/2000	78	X			
		PST_ERS_T494_F2781_CL001_POTENZA	10/07/1992-04/12/2000	80	X			
		PST_ERS_T494_F2799_CL001_CAPACCIO	10/07/1992-04/12/2000	78	X			
ENVISAT	Ascending	PST2009_ENVISAT_T86_F816_CL001_FOGGIA	04/05/2003-11/07/2010	39	X			
		PST2009_ENVISAT_T86_F798_CL001_POTENZA	04/05/2003-11/07/2010	42	X			
		PST2009_ENVISAT_T129_F801_CL001_SORRENTO	13/11/2002-14/07/2010	65	X	X	X	X
		PST2009_ENVISAT_T129_F801_CL002_CAPRI	13/11/2002-14/07/2010	65	X			
		PST2009_ENVISAT_T129_F801_CL003_ISCHIA	13/11/2002-14/07/2010	65	X			
		PST2009_ENVISAT_T358_F801_CL001_SALERNO	29/11/2002-30/07/2010	51	X			
		PST2009_ENVISAT_T358_F819_CL001_BENEVENTO	29/11/2002-30/07/2010	52	X	X		
		PST2009_ENVISAT_T129_F819_CL001_CASERTA	13/11/2002-14/07/2010	60	X	X		
ENVISAT	Descending	PST2009_ENVISAT_T36_F2781_CL001_NAPOLI	05/06/2003-03/06/2010	40	X	X		
		PST2009_ENVISAT_T308_F2769_CL001_SORA	02/09/2003-22/06/2010	36	X			
		PST2009_ENVISAT_T265_F2763_CL001_TERMOLI	08/03/2003-19/06/2010	43	X			
		PST2009_ENVISAT_T265_F2781_CL001_AVELLINO	08/03/2003-19/06/2010	49	X	X	X	X
		PST2009_ENVISAT_T36_F2763_CL001_ISERNIA	07/11/2002-03/06/2010	45	X			

Table A.2. List of the datasets from the PODIS_Tellus project archive exploited for the analyses (S = small, M = medium, L = large, D = detailed).

Sensor	Orbit Direction	Cluster	Period of acquisition	nr. of images	SCALE			
					S	M	L	D
RADARSAT	Ascending	ACERRA_RSAT_S3_A_T104_MARSEC_Regional	04/03/2003 - 5/09/2007	52	X			
		AGROPOLI_RSAT_S3_A_T204_MARSEC_Regional	28/04/2003 - 9/08/2007	51	X		X	
		NUSCO_RSAT_S3_A_T204_MARSEC_Regional	28/04/2003 - 2/09/2007	51	X		X	X
		ROFRANO_RSAT_S3_A_T204_MARSEC_Regional	28/04/2003 - 9/08/2007	51	X			
RADARSAT	Descending	ACERNO_RSAT_S3_D_T111_MARSEC_Regional	05/03/2003 - 23/08/2007	51	X			
		BISACCIA_RSAT_S3_D_T211_MARSEC_Regional	29/04/2003 - 0/08/2007	43	X			
		CAMEROTA_RSAT_S3_D_T211_MARSEC_Regional	9/04/2003 - 30/08/2007	43	X			
		SALERNO_RSAT_S3_D_T111_MARSEC_Regional	05/03/2003 - 3/08/2007	51	X		X	X

Table A.3. Characteristics of the COSMO-SkyMed dataset processed with SAR Tomography for the analysis at a detailed scale (S = small, M = medium, L = large, D = detailed).

Sensor	Orbit Direction	Period of acquisition	nr. of images	SCALE			
				S	M	L	D
COSMO-SkyMed	Descending	14/02/2010-17/02/2011	28				X

Acknowledgments

The authors wish to thank Italian Ministry of the Environment, Land and Sea and Campania Region for providing the PSInSAR data of the study area deriving from both the Italian Remote Sensing Extraordinary Plan and PODIS-Tellus project.

The authors also wish to thank the Italian Space Agency (ASI) for providing the COSMO-SkyMed dataset through the ASI AO Project ID2246.

REFERENCES

- Arangio, S., Calò, F., Di Mauro, M., Bonano, M., Marsella, M., Manunta M. 2013. An application of the SBAS-DInSAR technique for the assessment of structural damage in the city of Rome. *Structure and Infrastructure Engineering*, (ahead-of-print), 1-15, doi:10.1080/15732479.2013.833949
- Arnaud, A., Adam, N., Hanssen, R., Inglada, J., Duro, J., Closa, J., Eineder, M. 2003. ASAR ERS Interferometric phase continuity. In: *Proceedings International Geoscience and Remote Sensing Symposium*, Toulouse, 21-25 July, pp. 1133-1135.
- Ascione, L., Cascini, L., Sorbino, G., Peduto, D., Arena, L., Giordano, A., Spadea, S. 2011. Sull'analisi geotecnica e strutturale degli edifici afferenti al Piano PEEP in località Cariti nel Comune di Baronissi. Technical Report, not published (in Italian).
- Berardino, P., Fornaro, G., Lanari, R., Sansosti, E. 2002. A New Algorithm for Surface Deformation Monitoring Based on Small Baseline Differential SAR Interferograms. *IEEE Transactions on Geoscience and Remote Sensing*, 40(11), 2375-2383.
- Bianchini, S., Herrera, G., Mateos, R. M., Notti, D., Garcia, I., Mora, O., Moretti, S. 2013. Landslide activity maps generation by means of Persistent Scatterer Interferometry. *Remote Sensing*, 5(12), 6198-6222.
- Bjerrum, L. 1963. Allowable Settlement of Structures. *Proceedings of the 3rd European Conf. on Soil Mech. and Found. Engng*, Wiesbaden, 2, Brighton, England, 135-137.
- Borgia, A., Tizzani, P., Solaro, G., Manzo, M., Casu, F., Luongo, G., Pepe, A., Berardino, P., Fornaro, G., Sansosti, E., Ricciardi, G.P., Fusi, N., Di Donna, G., Lanari, R. 2005. Volcanic spreading of Vesuvius, a new paradigm for interpreting its volcanic activity. *Geophysical Research Letters*, vol. 32, L03303.
- Boscardin, M.D., Cording, E.G. 1989. Building Response to Excavation Induced Settlement, *Journal of Geotechnical Engineering-ASCE*, 115, 1-21.
- Brefort, T. 2011. GMES Data Access Specifications of the Earth observation needs over the period 2011-2013, Commission européenne, B-1049 Bruxelles / Europese Commissie, B-1049 Brussel - Belgium. U:\Spacedoc\Policy\Data policy\EO data specifications under the delegation agreement\V1.8 (CR Awifs)\Data warehouse specificationV1 8 clean.doc
- Burd, H.J., Houlby, G.T., Augarde, C.E., Liu, G. 2000. Modelling tunnelling-induced settlement of masonry buildings. *Proceedings of the ICE (Institute of Civil Engineers) - Geotechnical Engineering*, 143(1), 7-29.
- Burland, J.B., Wroth, C.P. 1974. Settlement of buildings and associated damage. *SOA Review. Proc. Conf. Settlement of Structures*, Cambridge, Pentech Press, London, pp. 611-654.
- Calderhead, A.I., Therrien, R., Rivera, A., Martel, R., Garfias, J. 2011. Simulating pumping-induced regional land subsidence with the use of InSAR and field data in the Toluca Valley, Mexico. *Advances in Water Resources* 34, 83-97.
- Carnec, C., King, C., Massonnet, D. 1995. Measurement of land subsidence by means of differential S.A.R. Interferometry to sites of small extent. *Geophysical Research Letters* 23, 3579-3582.
- Carrara, A. 1983. A multivariate model for landslide hazard evaluation. *Mathematical Geology*, 15, 403-426.
- Cascini, L., Ferlisi, S., Fornaro, G., Lanari, R., Peduto, D., Zeni, G. 2006. Subsidence monitoring in Sarno urban area via multitemporal DInSAR technique. *International Journal of Remote Sensing*, 27, 1709-1716.
- Cascini, L., Ferlisi, S., Peduto, D., Arena, L., Fornaro, G. 2011a. Monitoraggio con tecniche satellitari di aree urbanizzate in subsidenza. *Proceedings of the XXIV Italian Geotechnical Congress on "Innovazione Tecnologica nell'Ingegneria Geotecnica"*. Naples, 22-24 June 2011 - Edizioni AGI – Vol 2 pp. 657-664
- Cascini, L., Ferlisi, S., Peduto, D., Di Nocera, S., Fornaro, G., Serafino F. 2007a. A land subsidence study via DInSAR technique over large urbanised areas. *Proceedings of the Urban Remote Sensing Joint Event*. Paris 11-13 April, pp. 1-7, DOI:10.1109/URS.2007.371877
- Cascini, L., Ferlisi, S., Peduto, D., Fornaro, G. 2011b. The use of DINSAR techniques to analyse ground deformations and related effects to buildings. In "Deformation Characteristics of Geomaterials" (Ed. by Chung C., Kim H., Lee J., Jung Y., Kim D.), *Proceedings of the Fifth International Symposium on*

- Deformation Characteristics of Geomaterials. 1-3 September 2011, Seoul (Corea del Sud). Hanrimwon Co., Ltd. Edition. Vol. n. 2, pp. 1239-1246.
- Cascini, L., Ferlisi, S., Peduto, D., Fornaro, G., Manunta, M. 2007b. Analysis of a subsidence phenomenon via DInSAR data and geotechnical criteria. *Italian Geotechnical Journal*, XLI(4), 50-67.
- Cascini, L., Fornaro, G., Peduto, D. 2009. Analysis at medium scale of low-resolution DInSAR data in slow-moving landslide affected areas. *ISPRS Journal of Photogrammetry and Remote Sensing*, 64(6), 598-611.
- Cascini, L., Fornaro, G., Peduto, D. 2010. Advanced low- and full resolution DInSAR map generation for slow-moving landslide analysis at different scales. *Engineering Geology*, 112, 29-42.
- Cascini, L., Peduto, D., Arena, L., Fornaro, G. 2012. L'importanza di un protocollo nell'impiego di tecniche satellitari DInSAR. *Atti dell'Incontro Annuale dei Ricercatori di Ingegneria Geotecnica – IARG 2012*. Padova, 2-4 luglio 2012, p. 1-7, Rubano (PD):Grafiche Turato Edizioni (on CD-ROM) (in Italian)
- Cascini, L., Peduto, D., Reale, D., Arena, L., Ferlisi, S., Verde, S., Fornaro, G. 2013. Detection and monitoring of facilities exposed to subsidence phenomena via past and current generation SAR sensors. *Journal of Geophysics and Engineering*, 10.6 (2013): 064001.
- Casu, F., Manzo, M., Lanari, R. 2006. A quantitative assessment of the SBAS algorithm performance for surface deformation retrieval from DInSAR data, *Remote Sensing of Environment*, 102(3-4), 195-210.
- Chatterjee, R.S., Fruneau, B., Rundant, J.P., Roy, P.S., Frison, P.-L., Lakhera, R.C., Dadhwal, V.K., Saha, R. 2006. Subsidence of Kolkata (Calcutta) City, India during the 1990s as observed from space by Differential Synthetic Aperture Radar Interferometry (D-InSAR) technique. *Remote Sensing of Environment*, 102(1-2), 176-185.
- Cigna, F., Osmanoglu, B., Dixon, T.H., De Mets, C., Wdowinski, S. 2012. Monitoring land subsidence and its induced geological hazard with Synthetic Aperture Radar Interferometry: A case study in Morelia, Mexico. *Remote Sensing of Environment*, 117, 146-161.
- Cinque, A., Alinaghi, H.H., Laureti, L., Russo, F. 1987. Osservazioni preliminari sull'evoluzione geomorfologia della piana del Sarno (Campania, Appennino Meridionale). *Geografia Fisica e Dinamica Quaternaria*, 10, 161-174 (in Italian).
- Cocco, E., De Magistris, M.A., Bentivoglio, C., Iacone, Y., Serpico, M. 1993. Processi erosivi, opere di difesa e riequilibrio dei litorali in Campania. *La difesa dei litorali in Italia*, Edizioni delle Autonomie, 34, 175-194.
- Colesanti, C., Ferretti, A., Novali, F., Prati, C., Rocca F. 2003. SAR Monitoring of progressive and seasonal round deformation using the permanent scatterers technique, *IEEE Transactions on Geoscience and Remote Sensing*, 41, 1685-1701.
- Colesanti, C., Wasowski, J., 2006. Investigating landslides with space-borne Synthetic Aperture Radar (SAR) interferometry. *Engineering Geology*, 88 (3-4), 173-199.
- Corniello, A., Ducci, D., Trifuoggi, M., Rotella, M., Ruggieri G. 2010. Hydrology and Hydrogeochemistry of the plain between Mt. Massico and the river Volturno. *Italian Journal of Engineering Geology and Environment*, 1, 51-64.
- Costantini, M., Falco, S., Malvarosa, F., Minati F. 2008. A new method for identification and analysis of persistent scatterers in series of SAR images. *IEEE International Geoscience & Remote Sensing Symposium*, July 6-11, 2008, Boston, Massachusetts, USA, 449-452.
- Crosetto, M., Biescas, E., Duro J. 2008. Generation of advanced ERS and Envisat interferometric SAR products using the stable pointnetwork technique. *Photogrammetric Engineering and Remote Sensing*, 4, 443-450.
- Crosetto, M., Castillo, M., Arbiol, R. 2003. Urban subsidence monitoring using radar interferometry: Algorithms and validation. *Photogrammetric Engineering and Remote Sensing*, 69(7), 775-783.
- Crosetto, M., Crippa, B., Biescas, E. 2005. Early detection and in-depth analysis of deformation phenomena by radar interferometry. *Engineering Geology*, 79, 81-91.
- Del Ventisette, C., Ciampalini, A., Manunta, M., Calò, F., Paglia, L., Ardizzzone, F., Mondini, A.C., Reichenbach, P., Mateos, R.M., Bianchini, S., Garcia, I., Füsi, B., Deák, Z.V., Rádi, K., Graniczny, M., Kowalski, Z., Piatkowska, A., Przylucka, M., Retzo, H., Strozzi, T., Colombo, D., Mora, O., Sánchez,

- F., Herrera, G., Moretti, S., Casagli, N., Guzzetti, F. 2013. Exploitation of Large Archives of ERS and ENVISAT C-Band SAR Data to Characterize Ground Deformations. *Remote Sensing*, 5(8), 3896-3917.
- Fell, R., Corominas, J., Bonnard, Ch., Cascini, L., Leroi, E., Savage, W.Z. on behalf of the JTC-1 Joint Technical Committee on Landslides and Engineered Slopes. 2008. Guidelines for landslide susceptibility, hazard and risk zoning for land-use planning, Commentary. *Engineering Geology*, 102, 99-111.
- Ferretti, A., Prati, C., Rocca, F. 2000. Nonlinear Subsidence Rate Estimation Using Permanent Scatterers in Differential SAR Interferometry. *IEEE Transactions on Geoscience and Remote Sensing*, 38(5), 2202-2212.
- Ferretti, A., Prati, C., Rocca, F. 2001. Permanent scatterers in SAR interferometry. *IEEE Transactions on Geoscience and Remote Sensing*, 39(1), 8-20.
- Finno, R.J., Voss, F.T., Rossow, E., Blackburn, J.T. 2005. Evaluating Damage Potential in Buildings Affected by Excavations. *Journal of Geotechnical and Geoenvironmental Engineering*, 131(10), 1199-1210.
- Fornaro, G., Pascazio, V. 2014. SAR Interferometry and Tomography: Theory and Applications. In *Academic Press Library in Signal Processing*, vol. 2, Communications and Radar Signal Processing Chennai, R. Chellapa and S. Theodoridis, Eds. New York, NY, USA: Academic, pp. 1034-1117.
- Fornaro, G., Pauciuolo, A., Serafino, F. 2007. Multipass SAR Processing for urbanized areas imaging and deformation monitoring at small and large scales. *Proceedings of the Urban Remote Sensing Joint Event*. Paris 11-13 April, pp. 1-7, DOI:10.1109/URS.2007.371879
- Fornaro, G., Reale, D., Serafino, F. 2009. Four-dimensional SAR imaging for height estimation and monitoring of single and double scatterers. *IEEE Transactions on Geoscience and Remote Sensing*, 47(1), 212-237.
- Fornaro, G., Reale, D., Verde, S. 2012. Potential of SAR for monitoring transportation infrastructures: an analysis with the multi-dimensional imaging technique. *Journal of Geophysics and Engineering*, 9 S1
- Fornaro, G., Reale, D., Verde, S. 2013. Bridge thermal dilation monitoring with millimeter sensitivity via multidimensional sar imaging. *IEEE Geoscience and Remote Sensing Letters*, 10, 677-681.
- Fornaro, G., Reale, D., Verde, S., Peduto, D., Arena, L., Ferlisi, S. 2014. Potentialities of the use of spaceborne radar systems in the monitoring of structures and infrastructures, 2014 IEEE Workshop on Environmental Energy and Structural Monitoring Systems (EESMS), Naples, 17-18 September 2014, pp. 69-72. doi: 10.1109/EESMS.2014.6923267, © 2014 IEEE
- Fornaro, G., Serafino, F., Lombardini, F. 2005. 3D multipass SAR focusing: Experiments with long-term spaceborne data. *IEEE Transactions on Geoscience and Remote Sensing*, 43(4), 702-712.
- Fumagalli, A., Novali, F., Prati, C., Rocca, F., Rucci, A. 2011. A New Algorithm for Processing Interferometric Data-Stacks: SqueeSAR, *IEEE Transactions on Geoscience and Remote Sensing*, 49 (9), 3460-3470.
- Gabriel, K., Goldstein, R.M., Zebker, H.A. 1989. Mapping small elevation changes over large areas: differential interferometry. *Journal of Geophysical Research*, 94, 9183-9191.
- Galloway, D.L., Burgmann, R., Fielding, E., Amelung, F., Lacziak, R.J. 2000. Mapping recoverable aquifer-system deformation and land subsidence in Santa Clara Valley, California, USA, using space-borne synthetic aperture radar. *Proceedings of the 6th International Symposium on Land Subsidence (Ravenna, Italy)* (L. Carbognin, G. Gambolati and A. I. Johnson eds.), vol. 1, pp. 237-248.
- Gernhardt, S., Adam, N., Eineder, M., Bamler, R. 2010. Potential of very high resolution SAR for persistent scatterer interferometry in urban areas. *Annals of GIS*, 16(2), 103-111.
- Giannico, C., Ferretti, A., Alberti, S., Jurina, L., Ricci, M., Sciotti, A. 2012. Application of satellite radar interferometry for structural damage assessment and monitoring Life-Cycle and Sustainability of Civil Infrastructure Systems: IALCCE'12: Proc. of the 3rd Int. Symp. on Life-Cycle Civil Engineering (Vienna, Austria, 3-6 Oct.) ed A Strauss, D M Frangopol and K Bergmeister (Boca Raton, FL: CRC Press) 2012 2094-101.
- Guzzetti, F. 2005. Landslide hazard and risk assessment. PhD Thesis, Rheinischen Friedrich-Wilhelms-Universität Bonn.

- Haynes, M. 2000. Wide-area precision surveying of land subsidence from space using radar interferometry. *Procee. of the 6th Int. Symp. on Land Subsidence (Ravenna, Italy)* ed. L. Carbognin, G Gambolati and A. I. Johnson, vol. 2, pp. 213–8.
- Herrera, G., Fernandez-Merodo, J., Tomás, R., Cooksley, G., Mulas, J. 2009b. Advanced interpretation of subsidence in Murcia (SE Spain) using A-DInSAR data-modelling and validation. *Natural Hazards and Earth System Sciences*. 9, 647–661.
- Herrera, G., Tomás, R., Lopez-Sanchez, J. M., Delgado, J., Vicente, F., Mulas, J., Cooksley G., Sanchez M., Duro J., Arnaud A., Blanco P., Duque S., Mallorqui J.J., De la Vega-Panizo R., Monserrat O. 2009a. Validation and comparison of Advanced Differential Interferometry Techniques: Murcia metropolitan area case study. *ISPRS Journal of Photogrammetry and Remote Sensing*, 64(5), 501-512.
- Herrera, G., Tomás, R., Monells, D., Centolanza, G., Mallorquí, J.J., Vicente, F., Navarro, V.D., Lopez-Sanchez, J.M., Sanabria, M., Cano, M., Mulas, J. 2010b. Analysis of subsidence using TerraSAR-X data: Murcia case study. *Engineering Geology*, 116, 284–295.
- Herrera, G., Tomás, R., Vicente, F., Lopez-Sanchez, J. M., Mallorquí, J. J., Mulas, J. 2010a. Mapping ground movements in open pit mining areas using differential SAR interferometry. *International Journal of Rock Mechanics and Mining Sciences*, 47(7), 1114-1125.
- Hooper, A., Zebker, H., Segall, P., Kampes, B. 2004. A new method for measuring deformation on volcanoes and other natural terrains using InSAR persistent scatterers. *Geophysical Research Letters*, 31, L23611.
- ISPRA (Istituto Superiore per la Protezione e la Ricerca Ambientale) (2012). Pericolosità di origine naturale. *Annale dei dati ambientali*, <http://annuario.isprambiente.it/>, last access: 25/01/2014 (in Italian)
- Jung, H.S., Lu, Z., Won, J.-S., Poland, M.P., Miklius, A. 2011. Mapping Three-Dimensional Surface Deformation by Combining Multiple-Aperture Interferometry and Conventional Interferometry: Application to the June 2007 Eruption of Kilauea Volcano, Hawaii. *Geoscience and Remote Sensing Letters, IEEE*, 8(1), 34-38, doi: 10.1109/LGRS.2010.2051793.
- Jurina, L., Ferretti, A. (2004). Un caso emblematico di un parcheggio interrato: diagnosi di un dissesto. *Progettare il sottosuolo, per un edificio sicuro Milano*, 6 maggio 2004 (in Italian)
- Kampes, B.M., Adam, N. 2005. The STUN algorithm for persistent scatterer interferometry. *Fringe 2005 Workshop*, Frascati, Italy.
- Kim, S.W., Wdowski, S., Dixon, T.H., Amelung, F., Won, J. Kim, J. 2008. InSAR -based mapping of surface subsidence in Mokpo City, Korea, using JERS-1 and ENVISAT SAR data. *Earth Planets Space*, 60, 453-461.
- Kircher, M., Roth, A., Adam, N., Kampes, B.M., Neugebauer, H.J. 2003. Remote sensing observation of mining induced subsidence by means of differential SAR-interferometry. *Proceedings of the Geoscience and Remote Sensing Symposium, 2003. IGARSS '03, Toulouse, France, 21-25 July 2003, Vol 1*, pp. 209 – 211.
- Lanari, R., Berardino, P., Borgström, S., Del Gaudio, C., De Martino, P., Fornaro, G., Guarino, S., Ricciardi, G.P., Sansosti, E., Lundgren P. 2004a. The use of IFSAR and classical geodetic techniques for caldera unrest episodes: application to the Campi Flegrei uplift event of 2000. *Journal of Volcanology and Geothermal Research*, 247-260.
- Lanari, R., Mora, O., Manunta, M., Mallorqui, J.J., Berardino, P., Sansosti, E. 2004b. A Small Baseline Approach for Investigating Deformations on Full Resolution Differential SAR Interferograms. *IEEE Transaction on Geoscience and Remote Sensing*, 42 (7), 1377-1386.
- Lombardini, F. 2005. Differential tomography: a new framework for SAR interferometry *IEEE Transaction on Geoscience and Remote Sensing*, 43, 37-44.
- Lopez-Quiroz, P., Doing, M.P., Tupin, F., Briole, P., Nicolas, J.M. 2009. Time series analysis of Mexico City subsidence constrained by radar interferometry. *Journal of Applied Geophysics*, 69:1-15.
- Manzo, M., Ricciardi, G.P., Casu, F., Ventura, G., Zeni, G., Borgstrom, S., Berardino, P., Del Gaudio, C., Lanari, R. 2006. Surface deformation analysis in the Ischia Island (Italy) based on spaceborne radar interferometry. *Journal of Volcanology and Geothermal Research*, 151(4), 399-416.

- Massonnet, D., Feigl, K.L. 1998 Radar interferometry and its application to changes in the earth's surface. *Review of Geophysics*, 36(4), 441-500.
- MATTM, 2010. Piano Straordinario di Telerilevamento Ambientale (PSTA), Linee guida per l'analisi dei dati interferometrici satellitari in aree soggette a dissesti idrogeologici, Italian Ministry of the Environment and Protection of Land and Sea (MATTM), 108 pp.
- Meisina, C., Zucca, F., Notti, D., Colombo, A., Cucchi, A., Savio, G., Giannico, C., Bianchi, M. 2008. Geological Interpretation of PSInSAR Data at Regional Scale. *Sensors*, 8, 7469-7492.
- Milone, G., Scepti G. 2011. A Clustering Approach for Studying Ground Deformation Trends in Campania Region through PS-InSARTM Time Series Analysis. *Journal of Applied Sciences*, 11(4), 610-620.
- Mora, O., Mallorqui, J.J., Broquetas, A. 2003. Linear and nonlinear terrain deformation maps from a reduced set of interferometric SAR images. *IEEE Transactions on Geoscience and Remote Sensing*, 41, 2243-2253.
- Negulescu, C., Foerster, E. 2010. Parametric studies and quantitative assessment of the vulnerability of a RC frame building exposed to differential settlements. *Natural Hazards and Earth System Science*, 10(9), 1781-1792.
- Notti, D., Herrera, G., Bianchini, S., Meisina, C., García-Davalillo, J.C., Zucca, F. 2014. A methodology for improving landslide PSI data analysis. *International Journal of Remote Sensing*, 35(6), 2186-2214.
- Osmanoglu, B., Dixon, T.H., Wdowinski, S., Cabral-Cano, E., Jiang, Y. 2011. Mexico City subsidence observed with persistent scatterer InSAR. *International Journal of Applied Earth Observation and Geoinformation*, 13(1), 1-12.
- Peduto, D., Cascini, L., Arena, L., Sorbino, S. 2012. L'impiego dei dati PSInSAR per l'analisi dei cedimenti di edifici in area urbana: un caso di studio. In: *Proceedings of the Annual Meeting of Researchers in Geotechnics - IARG Padova, Italy, 2-4 July 2012 RUBANO (PD) Grafiche Turato Edizioni*, 1-6.
- Polshin, D.E., Tokar, R.A. 1957. Maximum allowable non-uniform settlement of structures. *Proceedings of the 4th International Conference on Soil Mechanics and Foundation Engineering*, London, Vol. 1, pp. 402-405.
- Raucoles, D., Maisons, C., Carnec, C., Le Mouelic, S., King, C., Hosford, S. 2003. Monitoring of slow ground deformation by ERS radar interferometry on the Vauvert salt mine (France). Comparison with ground-based measurement. *Remote Sensing of Environment*, 88, 468-478.
- Reale, D., Fornaro, G., Pauciuolo, A., Zhu, X., Bamler, R. 2011a. Tomographic imaging and monitoring of buildings with very high resolution SAR data. *IEEE Geoscience and Remote Sensing Letters*, 8, 661-665.
- Reale, D., Nitti, D.O., Peduto, D., Nutricato, R., Bovenga, F., Fornaro G. 2011. Post-seismic deformation monitoring with the COSMO/SKYMED constellation. *IEEE Geoscience and Remote Sensing Letters*, 8, 696-700.
- Risknat Project 2012. Le tecniche radar interferometriche nella pianificazione territoriale, KC Edizioni, Genova, Italy, 188 pp.
- Saeidi, A., Deck, O., Verdel, T. 2012. Development of building vulnerability functions in subsidence regions from analytical methods. *Géotechnique*, 62(2), 107-120
- Sanabria, M.P., Guardiola-Albert, C. Tomás, R., Herrera, G., Prieto, A., Sánchez, H., Tessitore, S. 2014. Subsidence activity maps derived from DInSAR data: Orihuela case study. *Natural Hazards and Earth Science Systems*, 14, 1341-1360.
- Santoro, U. 2001. Relazione geologica per la costruzione di un fabbricato sociale per civili abitazioni. Technical Report, not published (in Italian).
- Schack, L., Soergel, U. 2014. Exploiting Regular Patterns to Group Persistent Scatterers in Urban Areas. *IEEE Journal of Selected Topics in Applied Earth Observations and Remote Sensing*, 7(10), 4177-4183.
- Skempton A.W., MacDonald D.H. 1956. Allowable settlement of buildings. *Proceedings of the ICE (Institute of Civil Engineers)*, Vol. 5, Pt. III, pp 727-768.

- Stramondo, S. Saroli, M., Tolomei, C., Moro, M., Doumaz, F., Pesci, A., Loddo, F., Baldi, P., Boschi, E. 2007. Surface movements in Bologna (Po Plain-Italy) detected by multitemporal DInSAR. *Remote Sensing of Environment*, 110, 304–316.
- Terrafirma 2013. Available at: <http://www.terrafirma.eu.com>, last access: 21 July 2014.
- Terranova, C., Iuliano, S., Matano, F., Nardò, S., Piscitelli, E. 2009. Note tecniche descrittive delle elaborazioni eseguite dal Progetto Tellus del PODIS PON ATAS 2000-2006 sui dati da interferometria differenziale SAR (PS-InSAR) della Regione Campania. Relazione finale di Progetto 79 pp., Napoli; <http://www.difesa.suolo.regione.campania.it/content/category/4/64/92/>.
- Tomás, R., Herrera, G., Delgado, J., López-Sánchez, J.M., Mallorquí, J., Mulas, J. 2010. A ground subsidence study base don DInSAR data: calibration of soil parameters and subsidence prediction in Murcia City (Spain), *Engineering Geology*, 111, 19-30.
- Tomás, R., Romero, R., Mulas, J., Marturià, J.J., Mallorquí, J.J., López-Sánchez, J. M., Herrera, G., Gutiérrez, F., González, P.J., Fernández Torres, J., Duque, S., Concha-Dimas, A., Cocksley, G., Castañeda del Álamo, C., Carrasco, D., Blanco, P. 2014. Radar interferometry techniques for the study of ground subsidence phenomena: a review of practical issues through cases in Spain. *Environmental Earth Sciences*, 71(1), 163-181.
- Trigila, A., Iadanza, C. 2007. Statistiche nazionali ed elaborazioni dati del Progetto IFFI. APAT (2007). Rapporto sulle frane in Italia. Il Progetto IFFI – Metodologia, risultati e rapporti regionali, Rapporti 78/2007 (in Italian).
- van Westen, C.J. 1993. Application of Geographic Information Systems to Landslide Hazard Zonation. PhD Dissertation Technical University Delft. ITCPublication Number 15, ITC, Enschede, The Netherlands, 245 pp.
- Vilardo, G., Ventura, G., Terranova, C., Matano, F., Nardo, S. 2009. Ground deformation due to tectonic, hydrothermal, gravity, hydrogeological, and anthropic processes in the Campania Region (Southern Italy) from permanent scatterers synthetic aperture radar interferometry. *Remote Sensing of Environment*, 113, 197-212.
- Wang, Y., Zhu, X., Shi, Y., Bamler, R. 2012. Operational TomoSARprocessing using TerraSAR-X high resolution spotlight stacks from multiple view angles. *Proceedings IEEE 2012 IGARSS Conference*, (Munich, Germany), pp. 7047-7050.
- Wang, Z., Liu, G., Cui, Q. 2009. Monitoring the coal mining subsidence in Jibei mine area using DInSAR technique. *ICIECS'09: Information Engineering and Computer Science*, pp 1–4.
- Wasowski, J., Bovenga, F. 2014. Investigating landslides and unstable slopes with satellite Multi Temporal Interferometry: Current issues and future perspectives. *Engineering Geology*, 174, 103-138.
- Wegmüller, U., Werner, C., Strozzi, T., Wiesman, A. 2005. ERS _ ASAR integration in the interferometric point target analysis. *Proceedings Fringe 2005 Workshop*, Frascati, Italy, 28 November-2 December.
- Yerro, A., Corominas, J., Monells, D., Mallorquí, J.J. 2014. Analysis of the evolution of ground movements in a low densely urban area by means of DInSAR technique. *Engineering Geology*, 170, 52-65.
- Zebker, H.A., Goldstein, R.M. 1986. Topographic mapping from interferometric synthetic aperture radar observations, *Journal of Geophysical Researches*, 91(B5), 4993-4999.
- Zhu, X. 2011. Very high resolution tomographic SAR inversion for urban infrastructure monitoring—a sparse and nonlinear tour. *Deutsche Geodätische Kommission, Reihe C, Nr 666* (Verlag der Bayerischen Akademie der Wissenschaften).
- Zhu, X., Bamler, R. 2010. Very high resolution spaceborne SAR tomography in urban environment. *IEEE Transaction on Geoscience and Remote Sensing*, 48, 4296-4308.

List of Figure captions

Figure 1. The available SAR sensors, the archives and the achievable resolutions.

Figure 2. General framework for the use of DInSAR data (modified after Cascini et al., 2012).

Figure 3. Flow chart of the analysis to be carried out at small scale.

Figure 4. Flow chart of the analysis to be carried out at medium scale.

Figure 5. Flow chart of the analysis to be carried out at large scale.

Figure 6. Flow chart of the analysis to be carried out at detailed scale.

Figure 7. Preliminary phase of the analysis at small scale: (a) digital terrain model; (b) slope angle map; (c) flat area map; (d) operative grid of analysis.

Figure 8. Map of moving areas referred to: (a) ERS-1/2; (b) ENVISAT; (c) RADARSAT-1; (d) the whole period of observation.

Figure 9. Map of the Subsiding Plain Index computed for the whole period of observation (1992-2010).

Figure 10. Advanced map of moving areas according to ERS-1/2 (a); (b) ENVISAT and (c) RADARSAT-1 for covered cells by both ascending and descending DInSAR data.

Figure 11. Analysis at medium scale: (a) map of the urbanised area dated 2001 with indication of evidence of movement for the period 1992-2001; (b) map of the urbanised area dated 2009 with indication of evidence of movement for the period 2003-2010 (Cascini et al., 2013); (c) map of the urbanised area dated 2001 with indication of evidence of movement for the whole period 1992-2010 (Cascini et al., 2013).

Figure 12. Analysis at medium scale: map of subsiding municipalities referring to the period (a) 1992-2001, (b) 2003-2010 and (c) 1992-2010.

Figure 13. (a) close-up view map of ERS PS distribution in the municipality of Sarno (Campania region, southern Italy); (b) moving cells; (c) damaged masonry building; (d) damaged reinforced concrete building.

Figure 14. Castel Volturno municipality: (a) ERS PS distribution for the period 1992-2001; (b) ENVISAT PS distribution for the period 2003-2010; (c) map of moving cells for the whole period of observation (1992-2010).

Figure 15. Analysis at large scale: (a) localization of the study area of Baronissi municipal territory in the Campania region; (b) an orthophoto dated 2000 before buildings' construction and ERS PS (1: data on ascending orbit, 2: data on descending orbit) distribution; (c) an orthophoto dated 2006 after buildings' construction and both RADARSAT PS (3: data on ascending orbit, 4: data on descending orbit) and ENVISAT PS (5: data on ascending orbit, 6: data on descending orbit) distributions.

Figure 16. Analysis at large scale over Baronissi municipality: map of horizontal and vertical velocities in the period 1993-2000 from ERS-1/2 data (a,b) and 2003-2007 from RADARSAT data (c,d) (modified after Peduto et al., 2012).

Figure 17. Analysis at large scale: (a) map of cumulative settlements (period 2003-2010) using the combination of RADARSAT and ENVISAT data projected along the vertical direction; (b) map of settlement gradient vectors (period 2003-2010); damages recorded to the buildings framed in blue (c) and in red (d).

Figure 18. Analysis at detailed scale for a building in Baronissi municipality: (a) map of cumulative settlements; (b) mean cumulative settlements computed along the sketched profile at different dates starting from 2003 for four of the five blocks composing the building; c) cracks to external stairs; d) cracks to outside pavement; e) cracks to infilled walls.

Figure 19. Analysis at detailed scale for a building in the suburbs of Naples city: distribution of (a) ERS and (b) ENVISAT data; (c) results of the analysis at medium scale over the whole period 1992–2010 according to ERS-ENVISAT data; (d) COSMO-SkyMed data distribution; (e) map of cumulative settlements derived from COSMO-SkyMed data; (f) cumulative settlement and angular distortion values along the profile sketched in Figure 19e; (g) damages recorded among different blocks of buildings.

Figure 1
[Click here to download high resolution image](#)

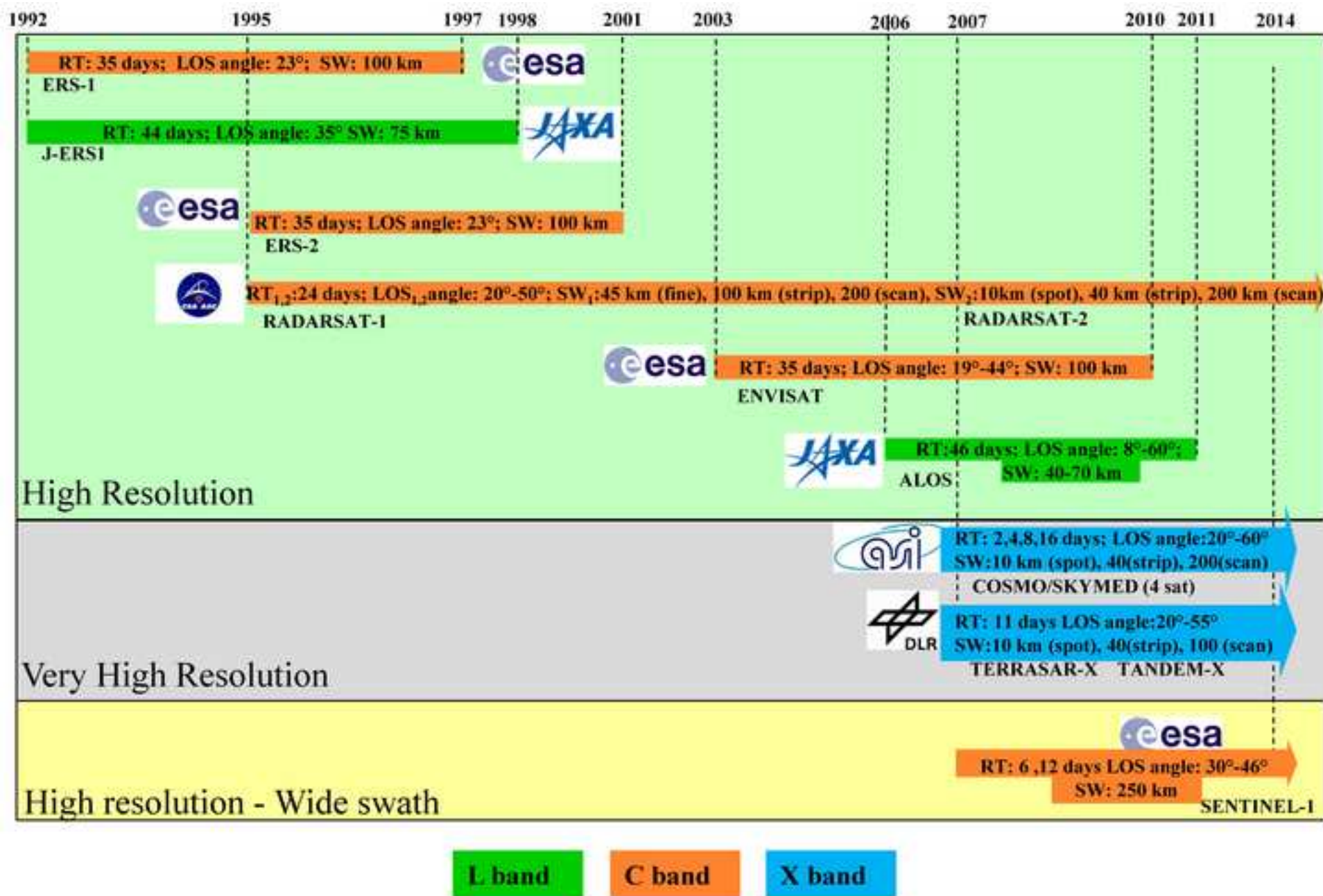


Figure 2
[Click here to download high resolution image](#)

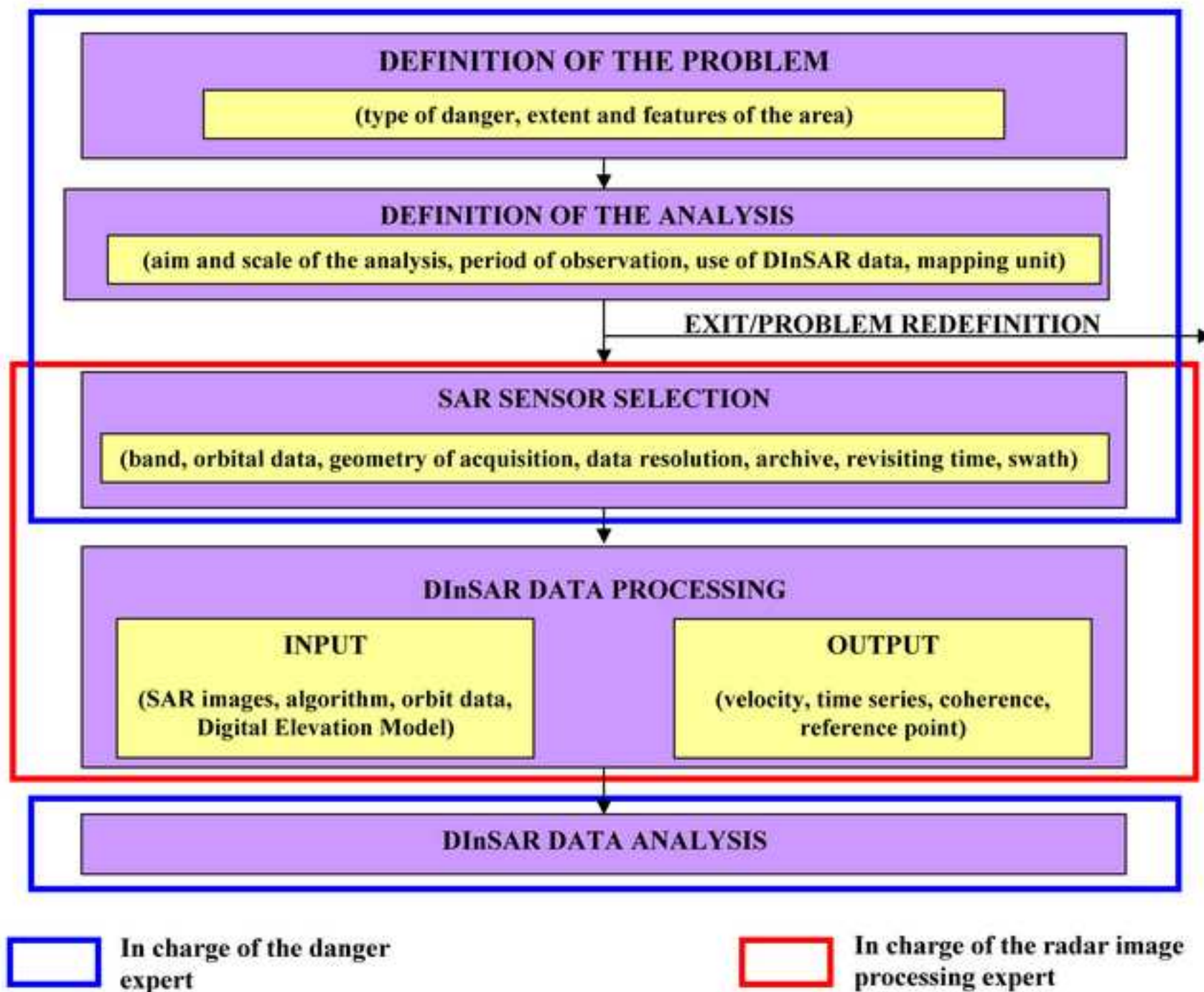


Figure 3
[Click here to download high resolution image](#)

INPUT	PROCEDURE	OUTPUT
<div>DIGITAL TERRAIN MODEL</div> <div>DInSAR DATA</div>	PRELIMINARY PHASE₀₀ <div>Masking areas with slope angles higher than 3°</div> <div>Selection of the operative grid according to the scale of the analysis</div> <div>DInSAR data treatment to account for the relative localization error</div>	<div>MAP OF FLAT AREAS</div> <div>OPERATIVE GRID OF ANALYSIS</div> <div>MAP OF DINSAR DATA</div>
	PHASE I₀₁ <div>Selection of ascending orbit DInSAR data intersecting the operative grid.</div> <div>Selection of descending orbit DInSAR data intersecting the operative grid</div> <div>Selection of the cells of the operative grid which contain both ascending and descending orbit DInSAR data</div>	<div>MAP OF COVERED CELL BY DInSAR DATA ON ASCENDING ORBIT</div> <div>MAP OF COVERED CELL BY DInSAR DATA ON DESCENDING ORBIT</div> <div>MAP OF COVERED CELL BY DInSAR DATA ON BOTH DESCENDING AND ASCENDING ORBIT</div>
<div>ALGORITHM FOR WEIGHTED VELOCITY COMPUTATION</div> <div>MOVEMENT THRESHOLD</div>	PHASE II₀₁ <div>Computation of the weighted velocity value on covered cell by DInSAR data on ascending orbit</div> <div>Computation of the weighted velocity value on covered cell by DInSAR data on descending orbit</div> <div>Clustering of moving cells on ascending and descending orbit</div>	<div>MAP OF MOVING CELLS ON ASCENDING ORBIT</div> <div>MAP OF MOVING CELLS ON DESCENDING ORBIT</div> <div><u>MAP OF MOVING AREAS</u></div>
<div>PLAIN BOUNDARIES</div>	PHASE III₀₁ <div>Computation of Subsiding Plain Index (Isp)</div>	<div><u>MAP OF SUBSIDING PLAINS</u></div>
<div>ALGORITHM FOR COMPUTATION OF VELOCITY ON BOTH VERTICAL AND EAST-WEST DIRECTION</div>	PHASE IV₀₁ <div>Computation of velocity values on vertical and East-West direction on covered cells by DInSAR data on both descending and ascending orbit.</div>	<div>MAP OF VERTICAL VELOCITY</div> <div>MAP OF EAST-WEST VELOCITY</div> <div><u>ADVANCED MAP OF MOVING AREAS</u></div>

Figure 4
[Click here to download high resolution image](#)

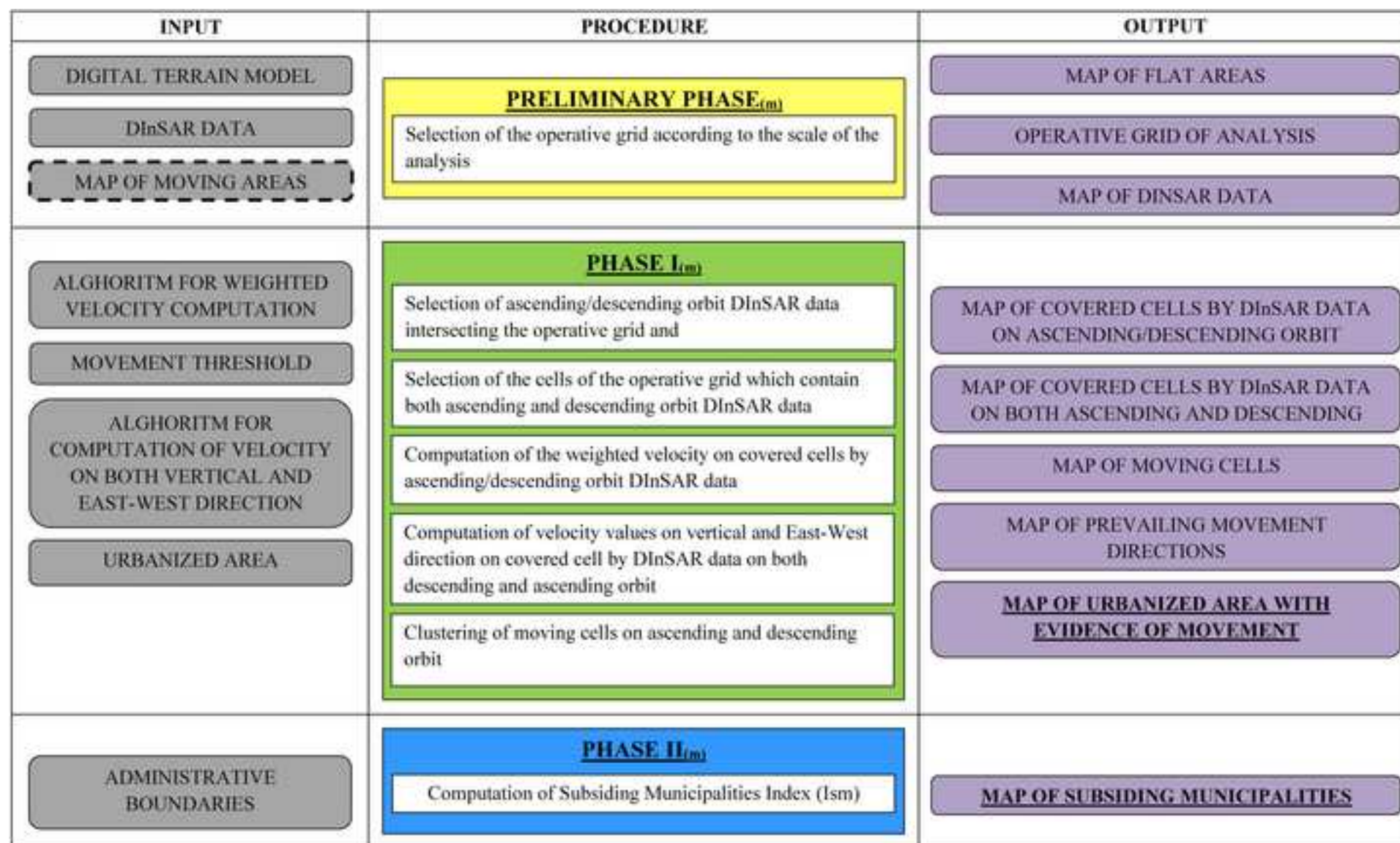


Figure 5
[Click here to download high resolution image](#)

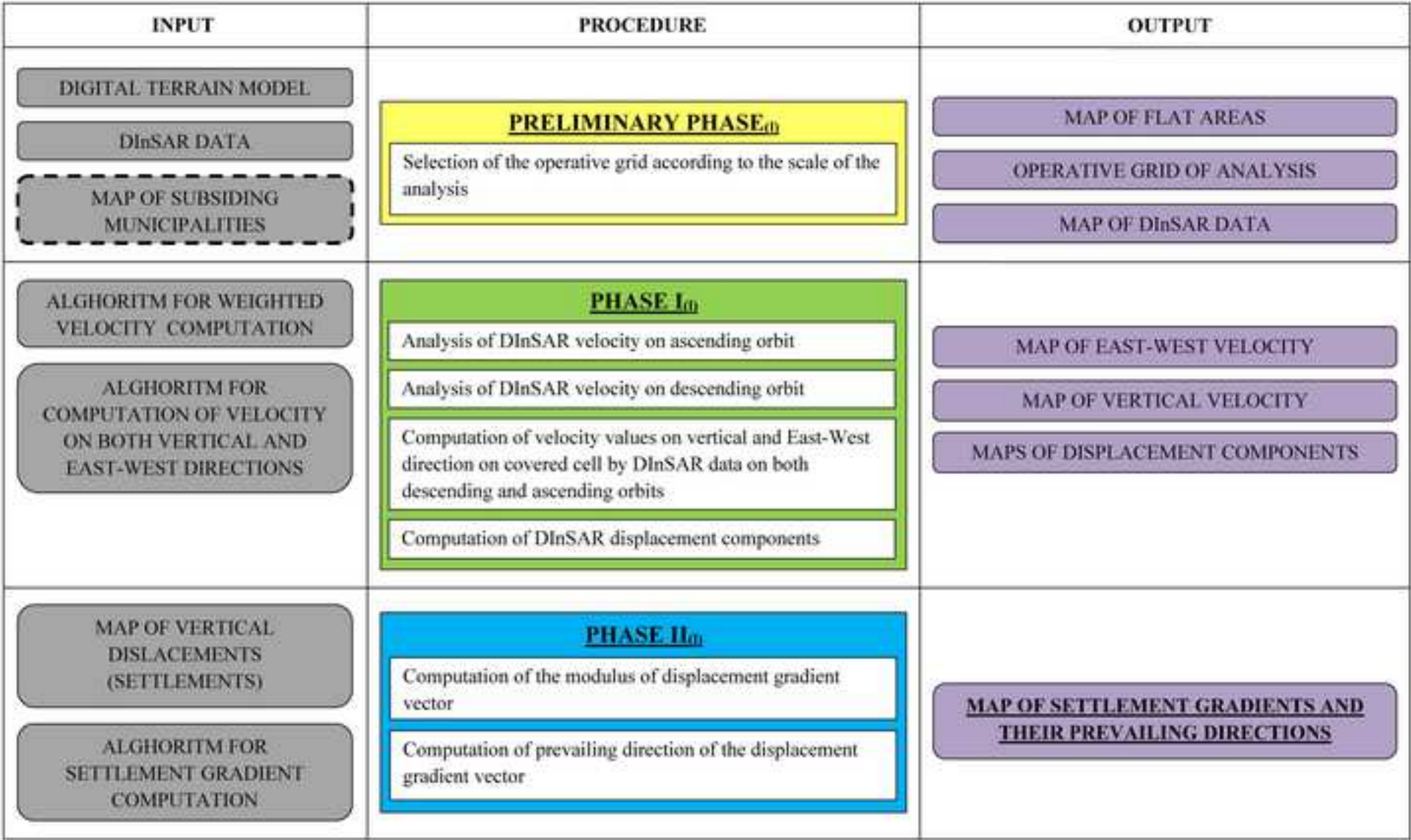


Figure 6
[Click here to download high resolution image](#)

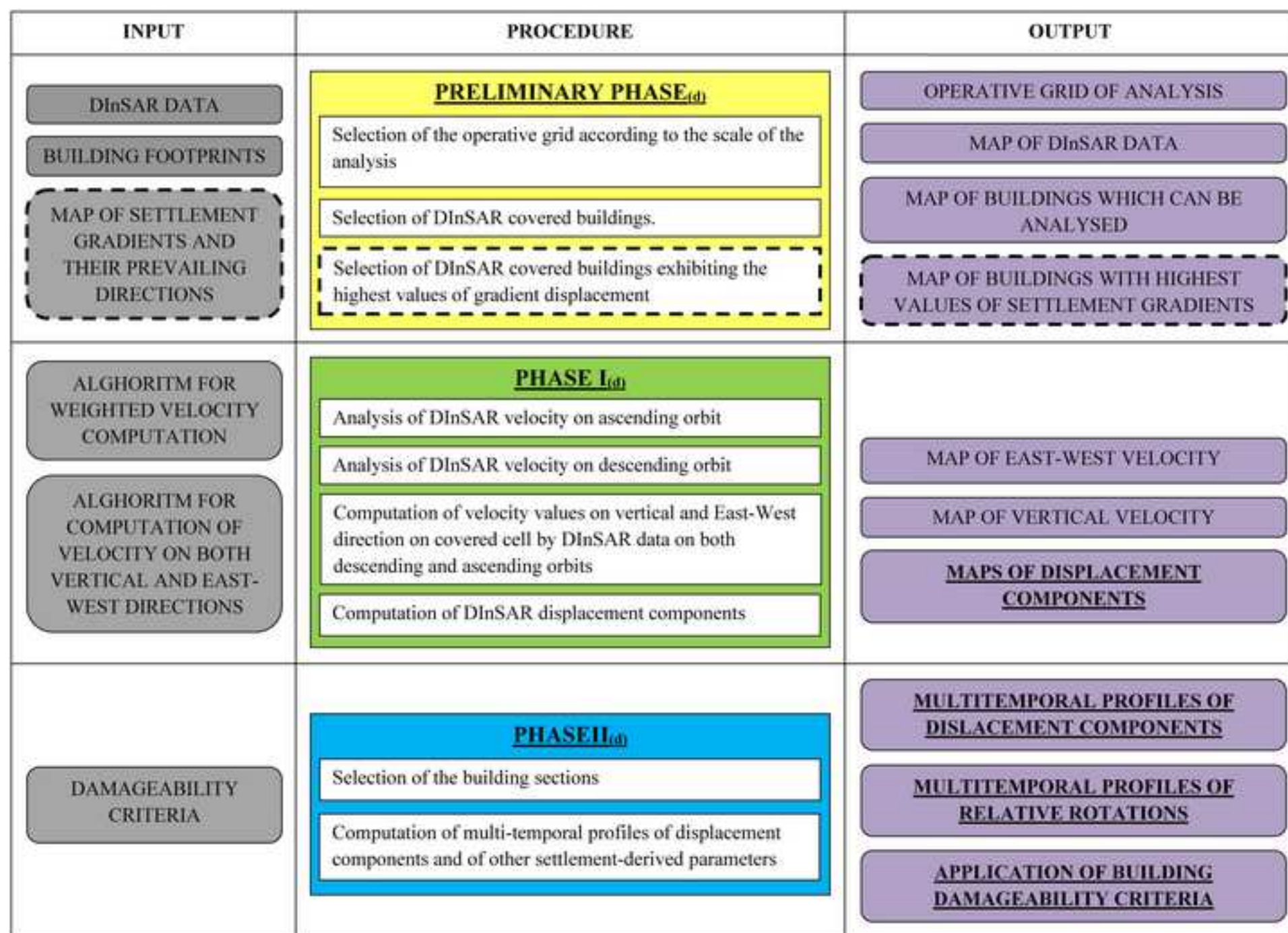


Figure 7
[Click here to download high resolution image](#)

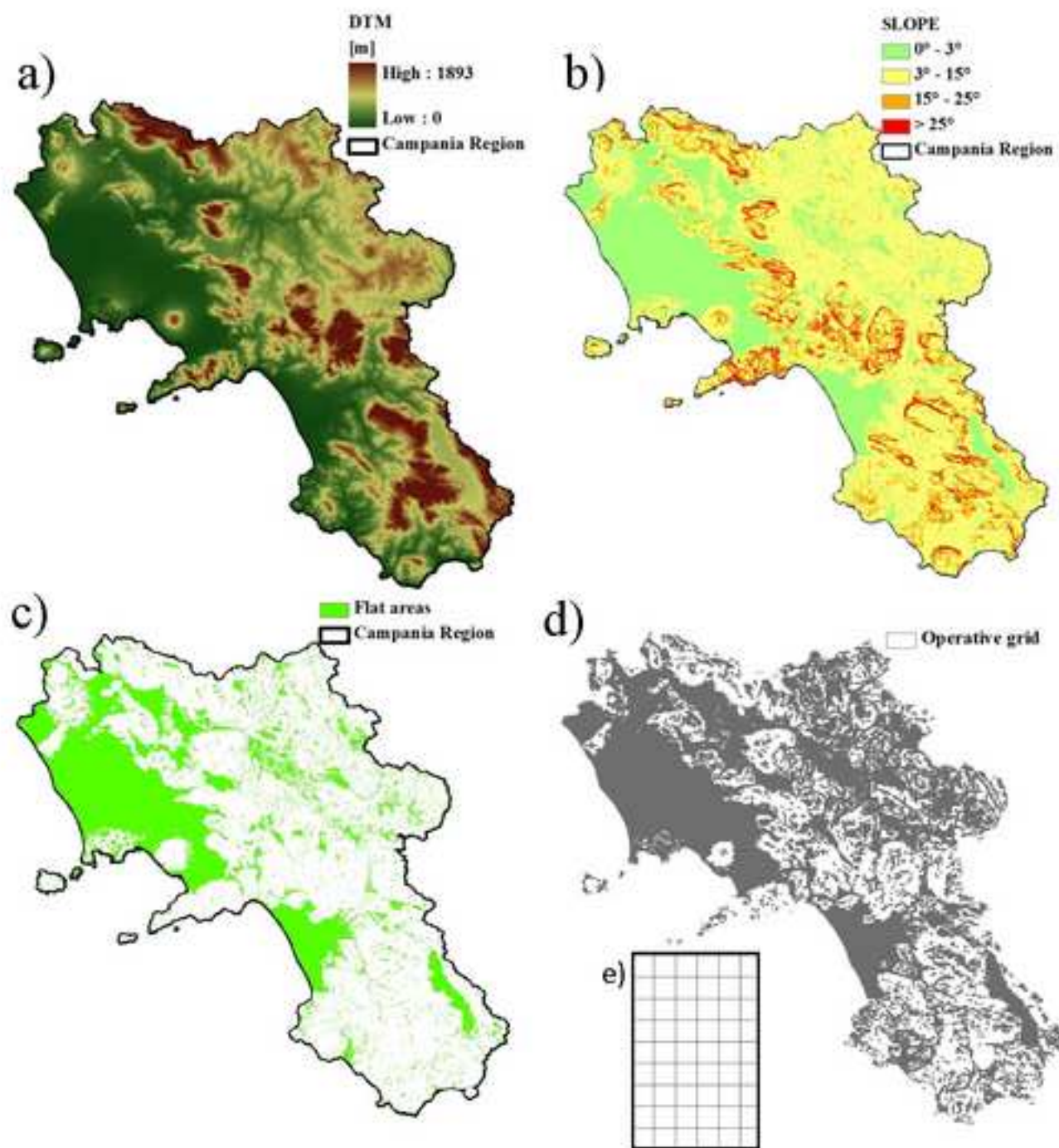


Figure 8
[Click here to download high resolution image](#)

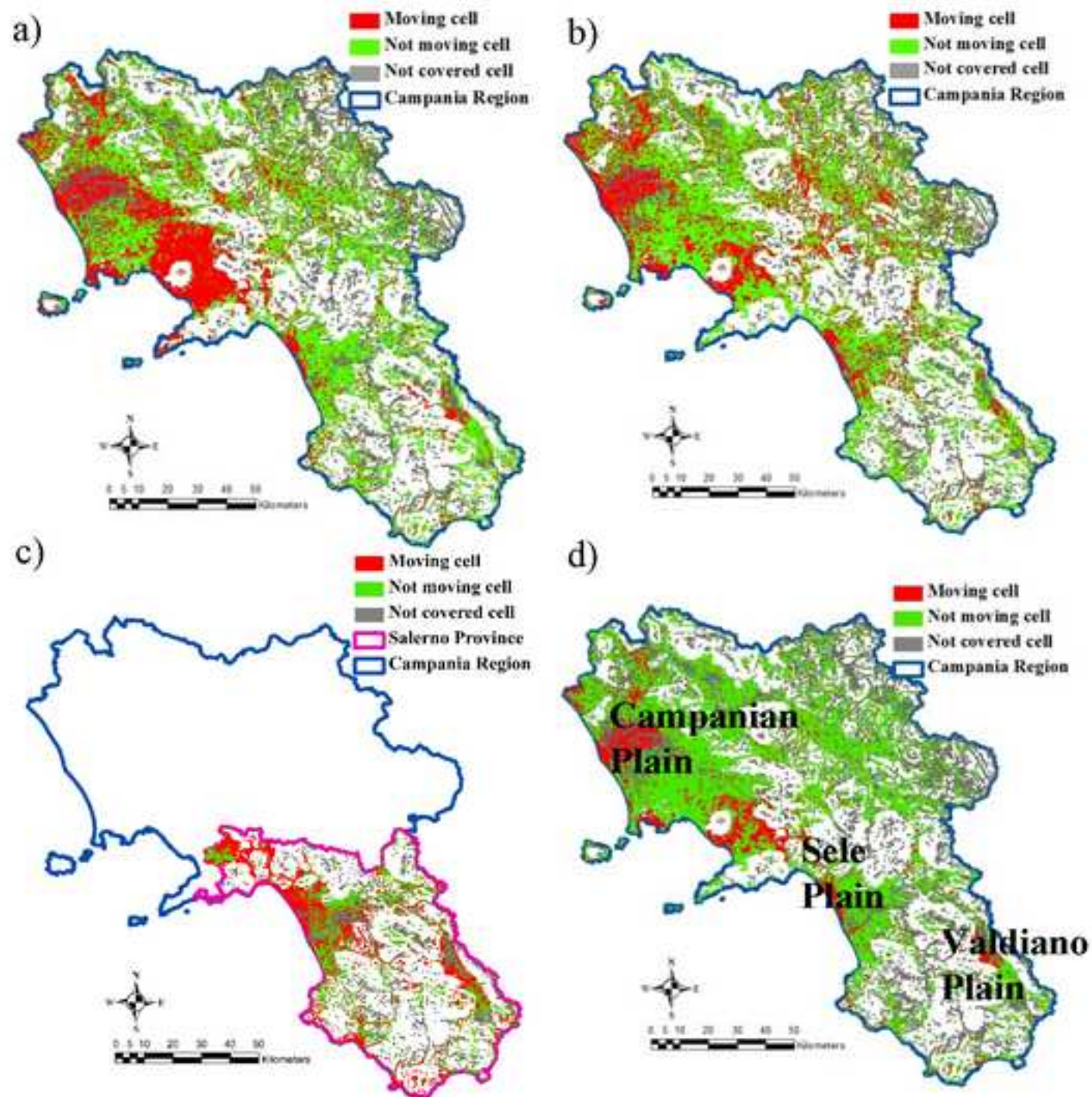


Figure 9

[Click here to download high resolution image](#)

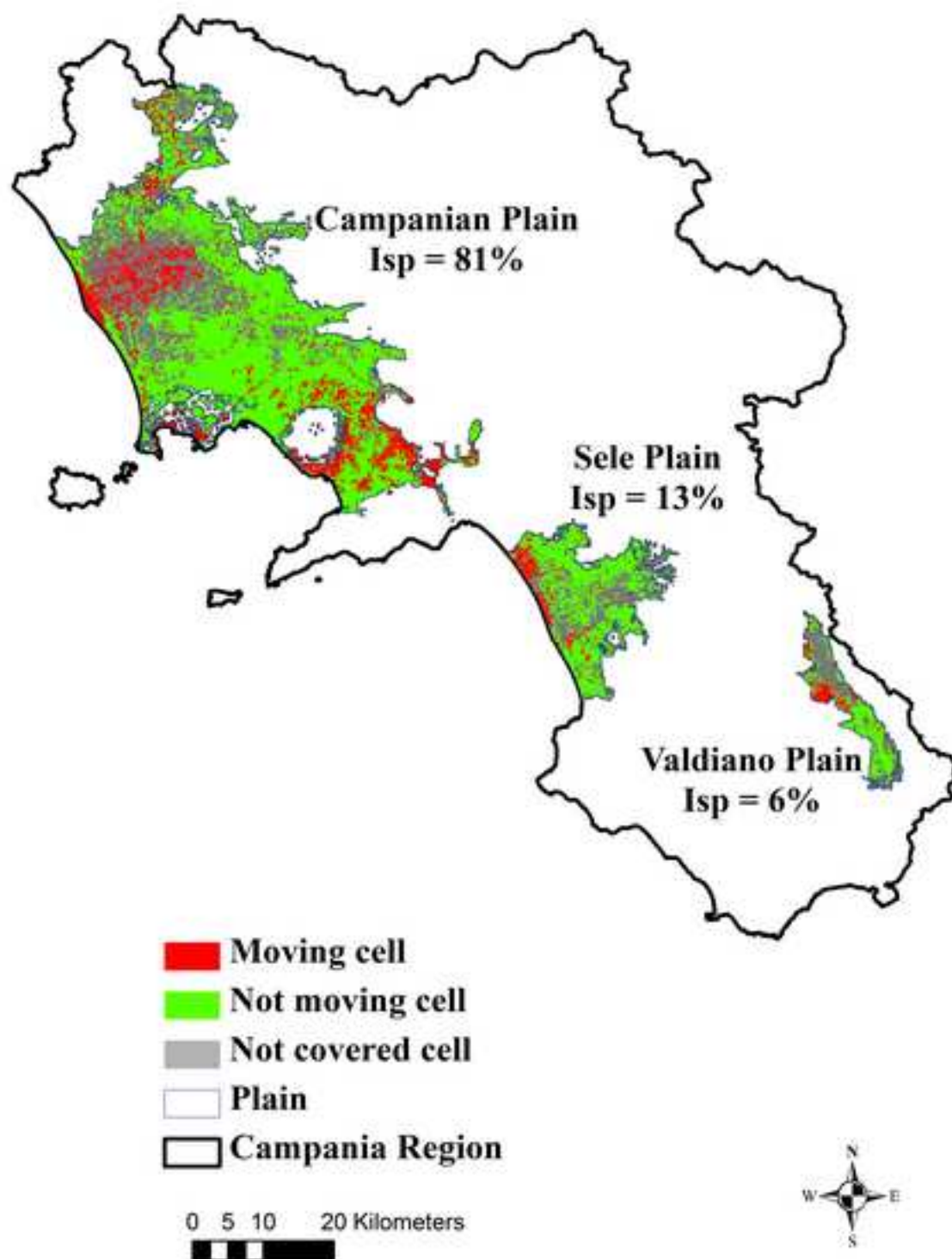


Figure 10

[Click here to download high resolution image](#)

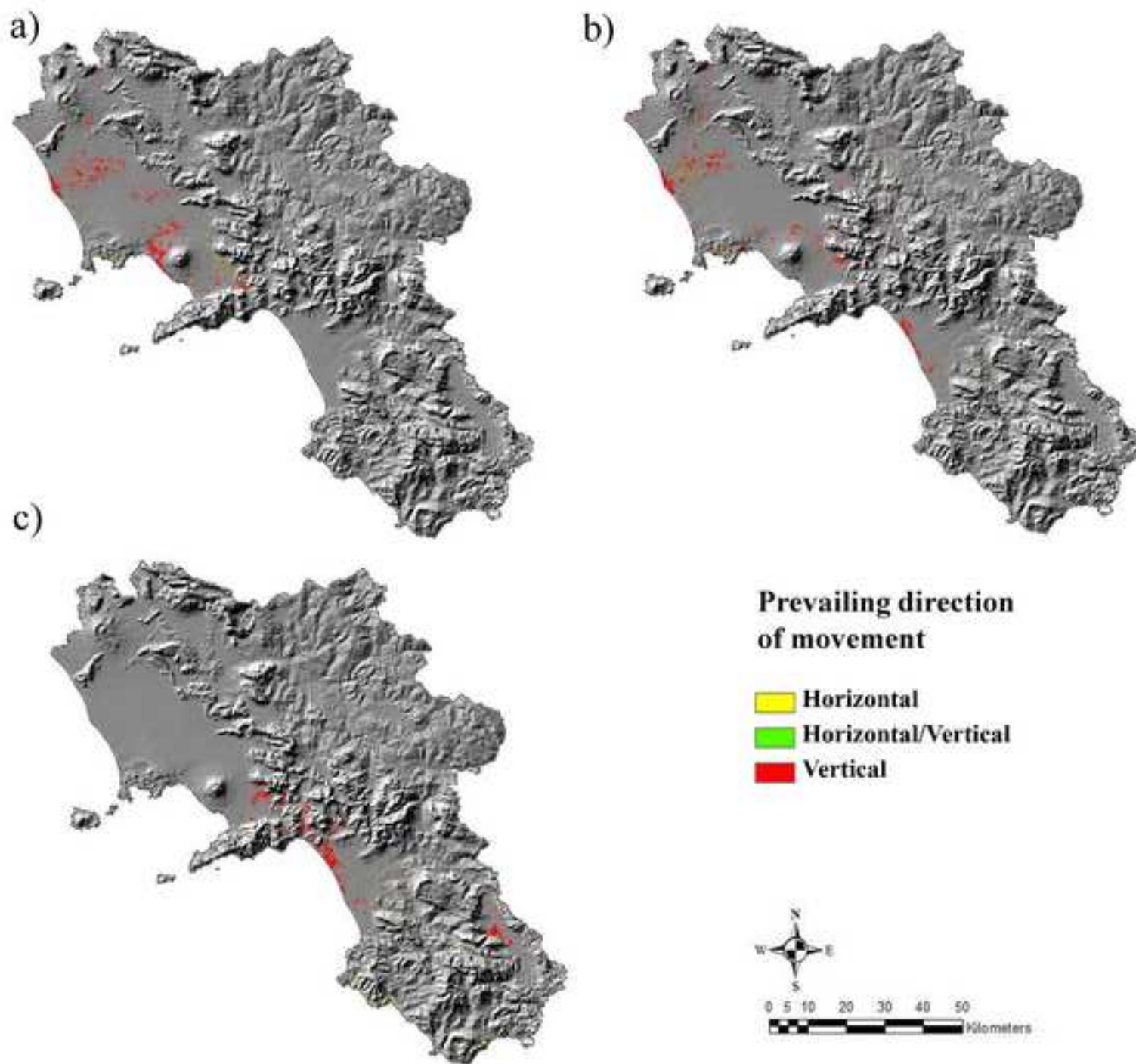


Figure 11

[Click here to download high resolution image](#)

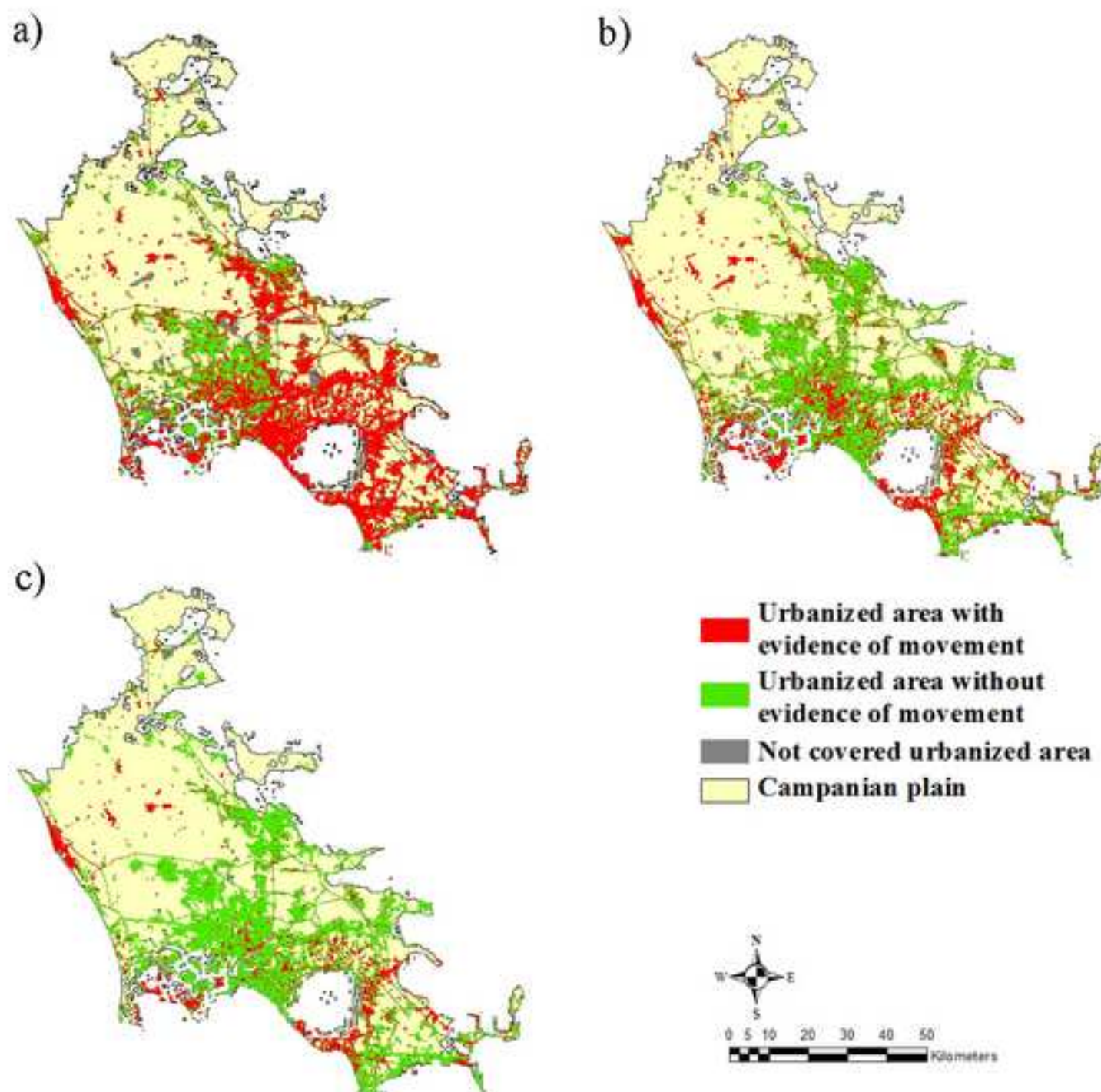


Figure 12
[Click here to download high resolution image](#)

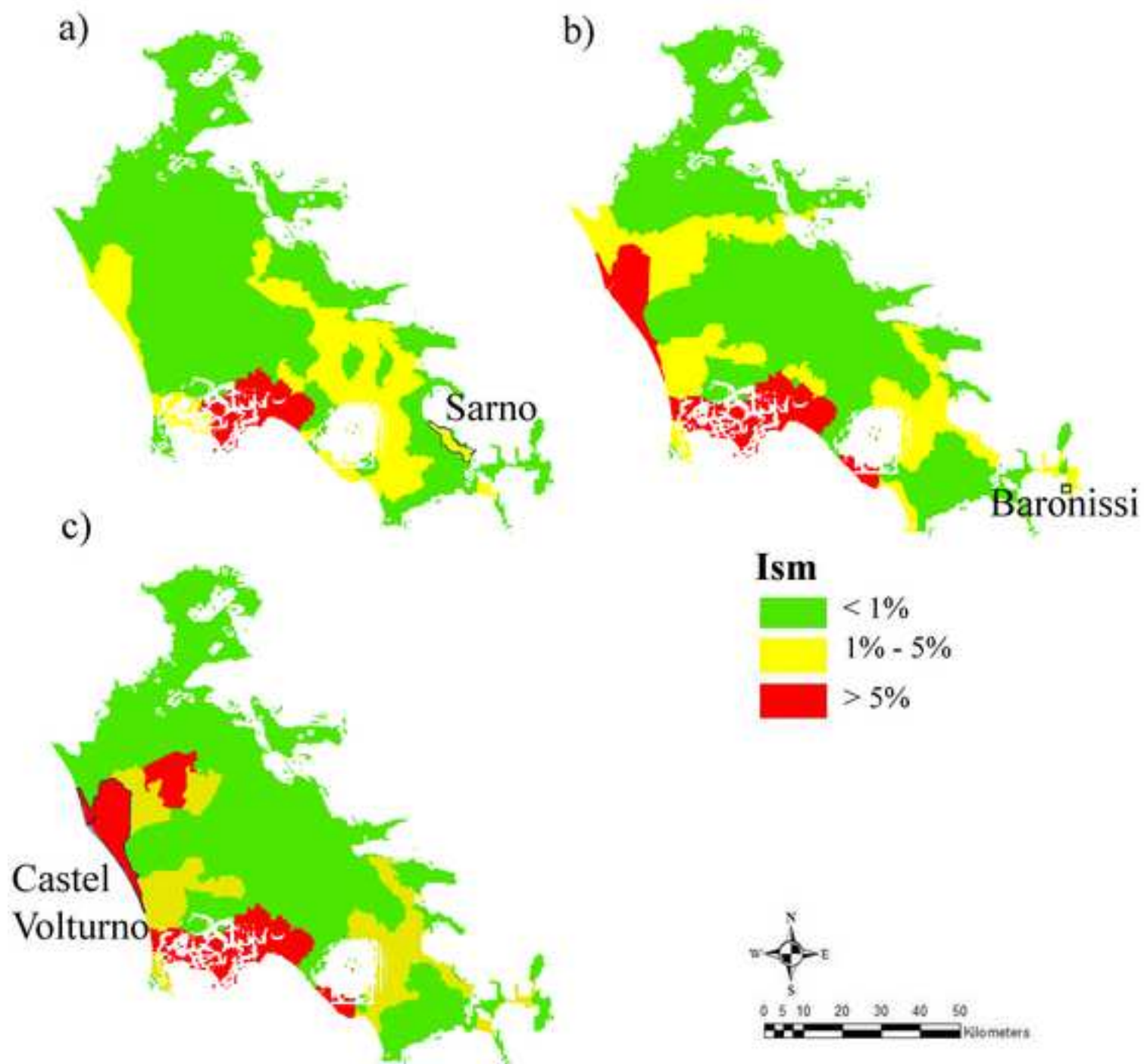


Figure 13
[Click here to download high resolution image](#)

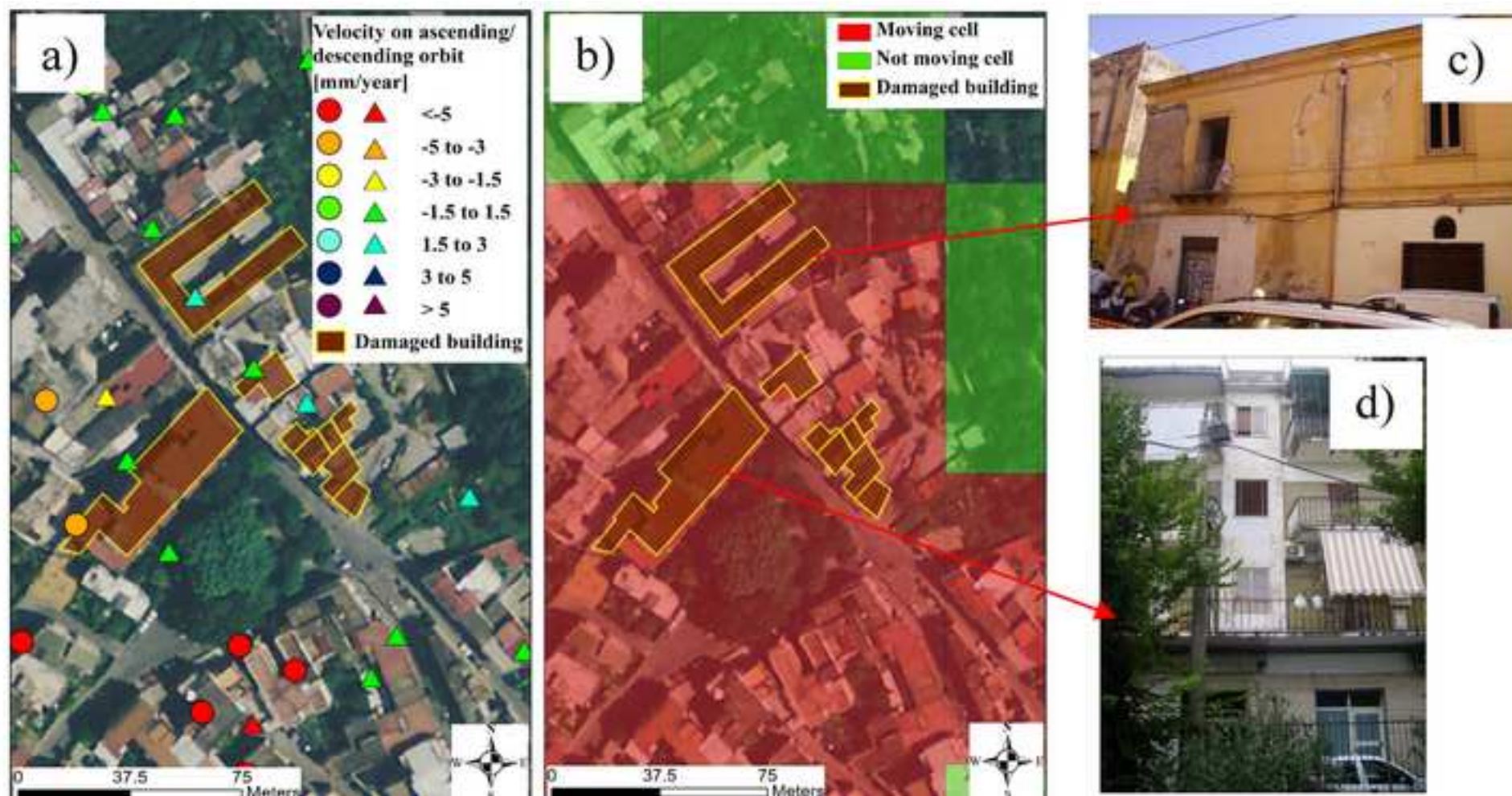


Figure 14
[Click here to download high resolution image](#)

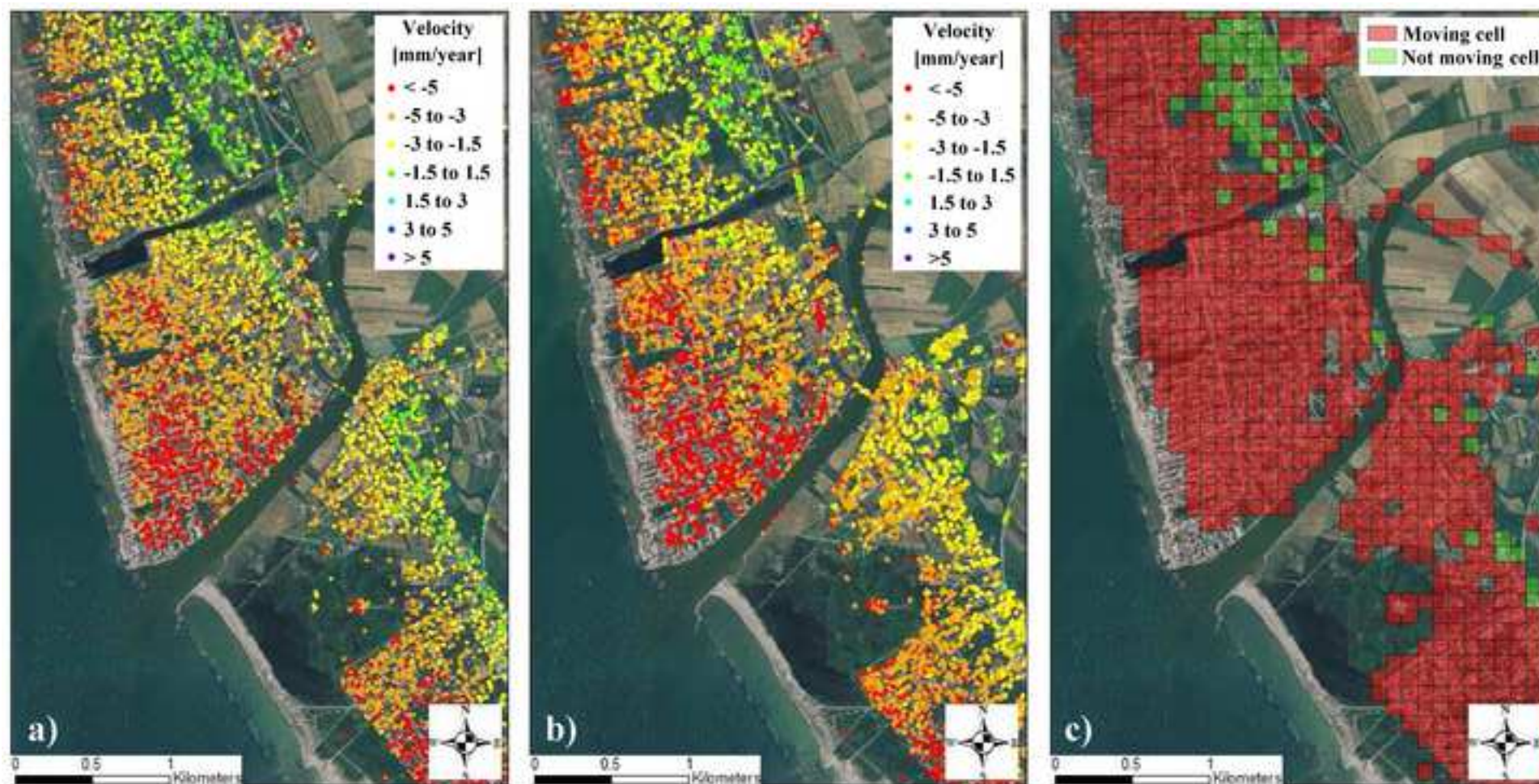
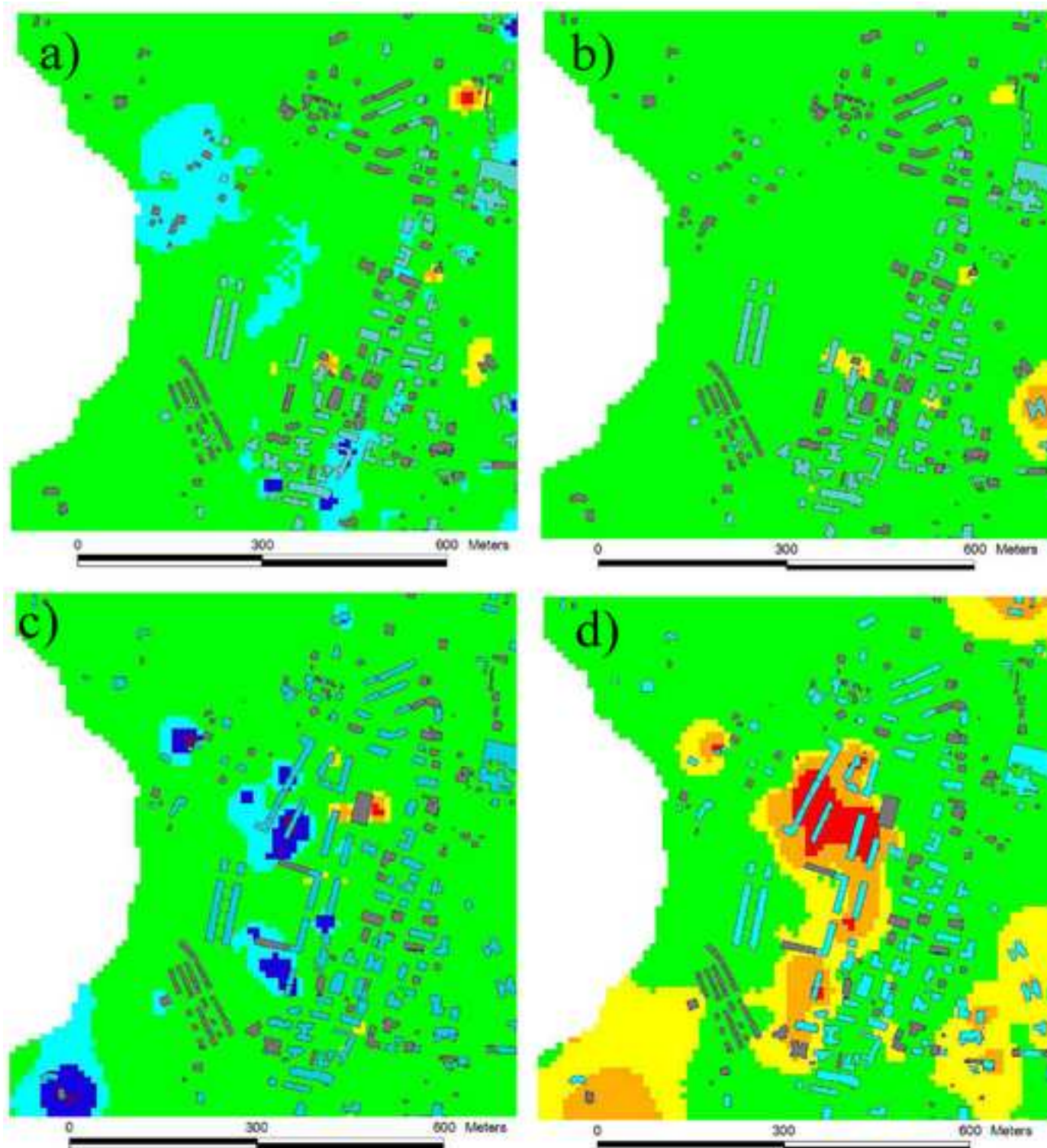




Figure 15
[Click here to download high resolution image](#)



Figure 16
[Click here to download high resolution image](#)



 Covered building
 Not covered building

Horizontal/vertical velocity [mm/year]

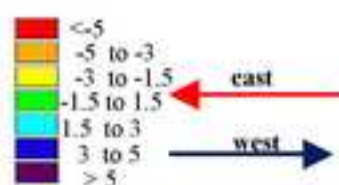


Figure 17
[Click here to download high resolution image](#)

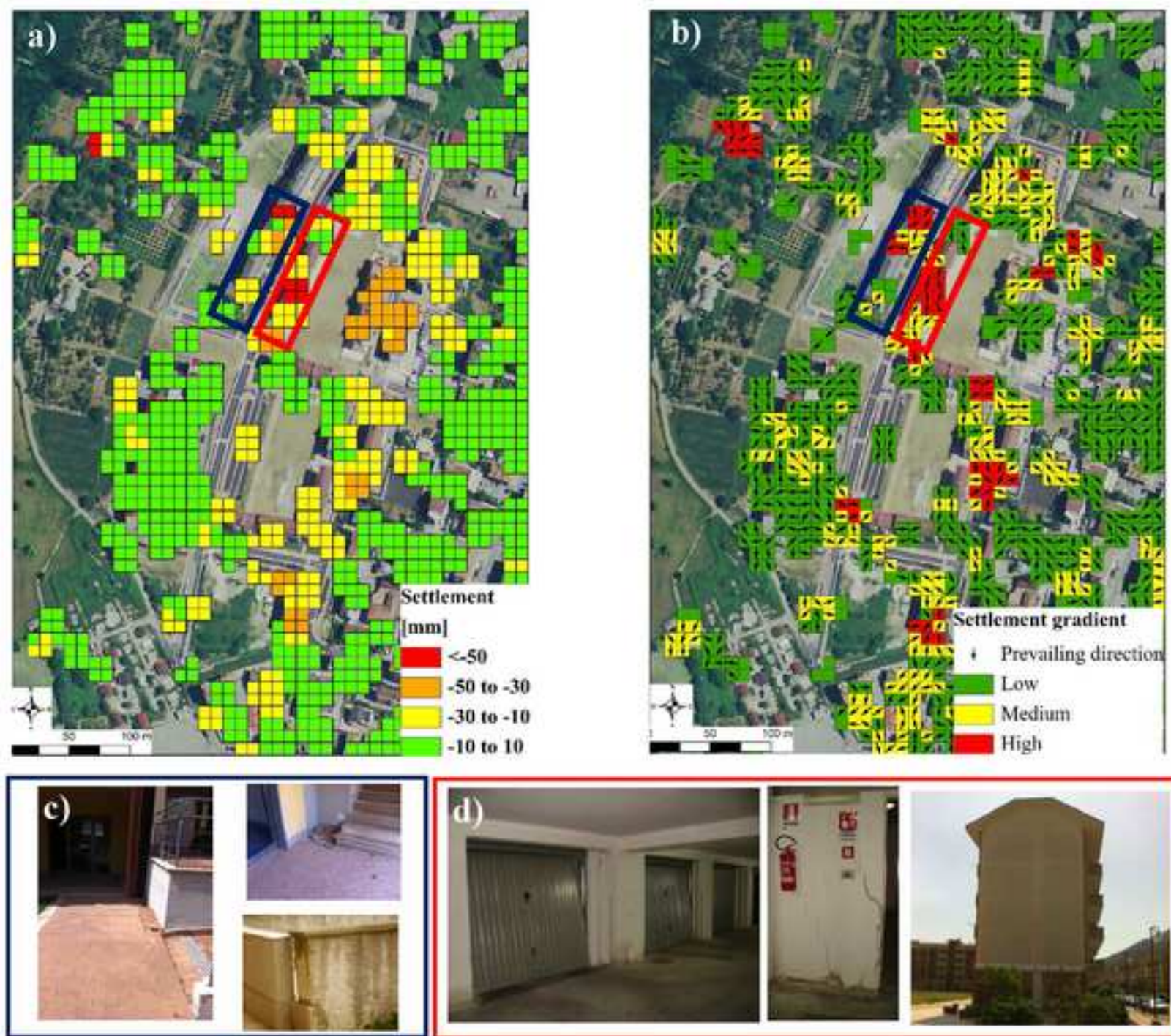


Figure 18
[Click here to download high resolution image](#)

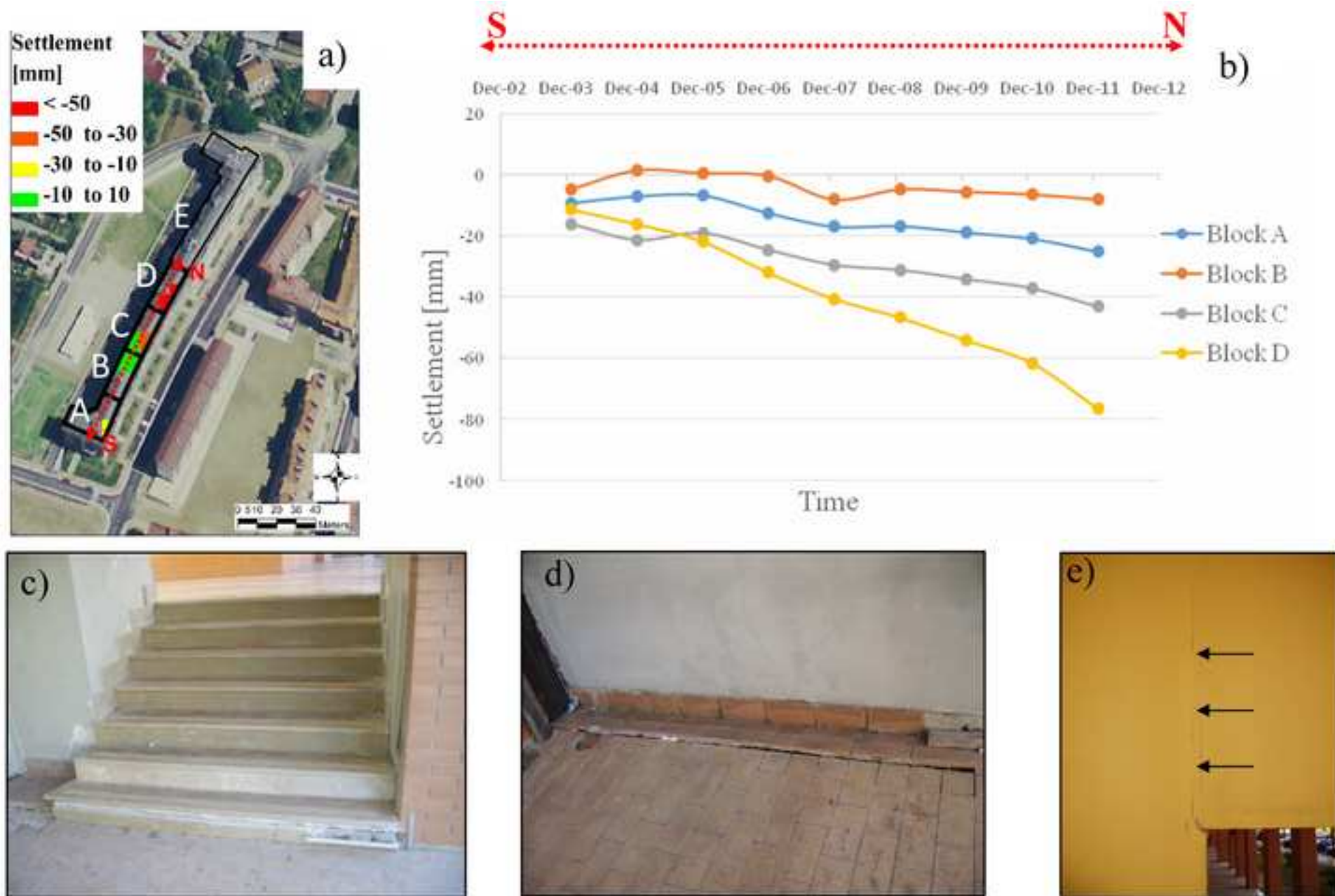


Figure 19
[Click here to download high resolution image](#)



Table 1. Examples of applications of DInSAR technique to subsidence analyses at different scales.

Case study	Causes	Scale	Sensor	Algorithm	Author
Piedmont region, Italy	External loads and water withdrawals; rock dissolution and consolidation of soft soils	Small	ERS-1/2	PSInSAR	Meisina et al. (2008)
Campania region, Italy	Tectonic, hydrothermal, gravity, hydrogeological and anthropic processes	Small	ERS-1/2	PSInSAR	Vilardo et al. (2009)
Catalonia, Spain	Salt mine	Medium	ERS	(DInSAR)	Crosetto et al. (2003)
Toluca Valley basin, Mexico	Water withdrawals	Medium	ERS-1, ENVISAT ASAR, RADARSAT-1	(D-InSAR)	Calderhead et al. (2010)
Campanian plain, Italy	Water withdrawals	Medium	ERS-1/2	ESD	Cascini et al. (2007a)
Murcia metropolitan area, Spain	Water withdrawals	Large	ERS-1, ENVISAT ASAR	SPN and CPT	Herrera et al. (2009)
			TerraSAR-X	CPT	Herrera et al. (2010)
Bologna, Italy	Water withdrawals and active tectonics	Large	ERS	SBAS	Stramondo et al. (2007)
Sarno, Italy	Water withdrawals	Large	ERS-1/2	ESD	Cascini et al. (2007b; 2011a)
Mexico City, Mexico	Water withdrawals	Large	ENVISAT	JPL/ CalTech Repeat Orbit Interferometry Package (ROI_PAC)	Lopez-Quiroz et al. (2009)
				PSI	Osmanoglu et al. (2011)
Mokpo City, Korea	Soil compaction	Large	JERS-1, ENVISAT	InSAR/ PSInSAR	Kim et al. (2008)
Calcutta City, India	Water withdrawals	Large	ERS	D-InSAR	Chatterjee et al. (2006)
Orihuela City, Spain	Water withdrawals	Large	ERS, ENVISAT	CPT	Tomás et al. (2010) Sanabria et al. (2014)
Súria, Spain	Underground mining activities	Large	ERS, ENVISAT	DInSAR	Yerro et al. (2014)
Rovigo, Italy	Underground construction	Detailed	ERS	PSInSAR	Jurina and Ferretti (2004)
Sarno, Italy	Water withdrawals	Detailed	ERS-1/2	SBAS	Cascini et al. (2007b; 2011b)
Rome, Italy	Consolidation process	Detailed	ERS-1/2, ENVISAT	SBAS	Arangio et al. (2013)

Table 2. Different scales of analysis of DInSAR data with indication of the size of the mapping unit and the objectives to be pursued.

SCALE	RANGE OF SCALES	SIZE OF MAPPING UNIT (e.g. cell) [m × m]	PURPOSES / EXAMPLES OF APPLICATION
SMALL	< 1:100,000	$\geq 100 \times 100$	Zoning of moving areas
MEDIUM	1:100,000 to 1:25,000	25 × 25 to 100 × 100	Inventory and ranking of affected municipalities
LARGE	1:25,000 to 1:5,000	5 × 5 to 25 × 25	Zoning of built-up areas where damage occurred or is likely to occur and analysis of damage severity
DETAILED	>1:5,000	$\leq 5 \times 5$	Detection of damaged /likely damaged buildings